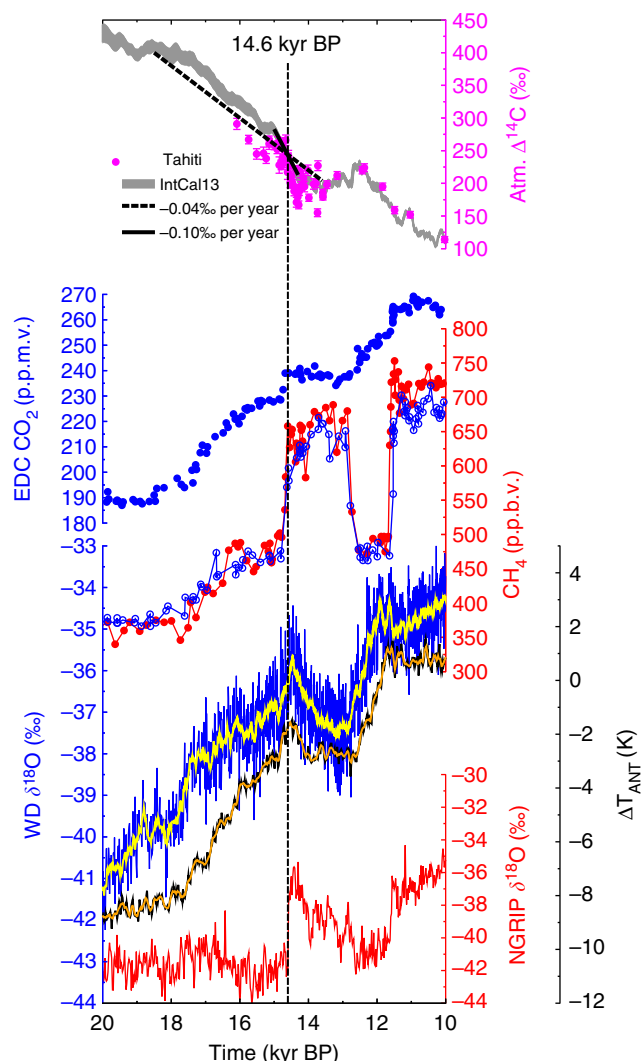# ARTICLE

DOI: 10.1038/ncomms6520   **OPEN**

Permafrost thawing as a possible source of abrupt carbon release at the onset of the Bølling/Allerød

Peter Köhler[1], Gregor Knorr[1,2] & Edouard Bard[3]

One of the most abrupt and yet unexplained past rises in atmospheric CO_2 (>10 p.p.m.v. in two centuries) occurred in quasi-synchrony with abrupt northern hemispheric warming into the Bølling/Allerød, $\sim 14,600$ years ago. Here we use a U/Th-dated record of atmospheric $\Delta^{14}C$ from Tahiti corals to provide an independent and precise age control for this CO_2 rise. We also use model simulations to show that the release of old (nearly ^{14}C-free) carbon can explain these changes in CO_2 and $\Delta^{14}C$. The $\Delta^{14}C$ record provides an independent constraint on the amount of carbon released (~ 125 Pg C). We suggest, in line with observations of atmospheric CH_4 and terrigenous biomarkers, that thawing permafrost in high northern latitudes could have been the source of carbon, possibly with contribution from flooding of the Siberian continental shelf during meltwater pulse 1A. Our findings highlight the potential of the permafrost carbon reservoir to modulate abrupt climate changes via greenhouse-gas feedbacks.

[1] Alfred-Wegener-Institut Helmholtz-Zentrum für Polar-und Meeresforschung (AWI), P.O. Box 12 01 61, D-27515 Bremerhaven, Germany. [2] School of Earth and Ocean Sciences, Cardiff University, Cardiff CF10 3AT, UK. [3] CEREGE, Aix Marseille University, CNRS, IRD, College de France, B.P. 80 Technopole de l'Arbois, 13545 Aix-en-Provence, France. Correspondence and requests for materials should be addressed to P.K. (email: Peter.Koehler@awi.de).

1

Changes in the global carbon cycle during the last deglaciation are so far not completely understood. However, based on the data and model-based interpretation, the emerging picture indicates that the rise in atmospheric CO_2 of ~45 p.p.m.v. during the first half of the deglaciation (~1 p.p.m.v. per century) was probably fuelled by the release of old, ^{13}C- and ^{14}C-depleted deep ocean carbon[1,2]. The processes responsible for CO_2 rise have changed dramatically with the beginning of the Bølling/Allerød (B/A) ~14,600 years before present (~14.6 kyr BP). Here the abrupt CO_2 rise recorded in the EPICA Dome C (EDC) ice core[3,4] was six times faster than before, about 10 p.p.m.v. in 180 years or ~6 p.p.m.v. per century (Fig. 1). Atmospheric CH_4 rose by 150 p.p.b.v. between 18.5 and 14.6 kyr BP and then by the same amount again, but within

centuries, around the onset of the B/A. The changes in both greenhouse gases (GHG) imply that a ratio of both changes $\Delta CH_4 / \Delta CO_2$ is a factor of five larger around 14.6 kyr BP than during the previous four millennia. Such a change in the ratio $\Delta CH_4 / \Delta CO_2$ might be the first indication that the wetlands identified[5] as the main contributor to the rapid rise in CH_4 at the onset of the B/A might also have contributed to the abrupt rise in CO_2 at that time.
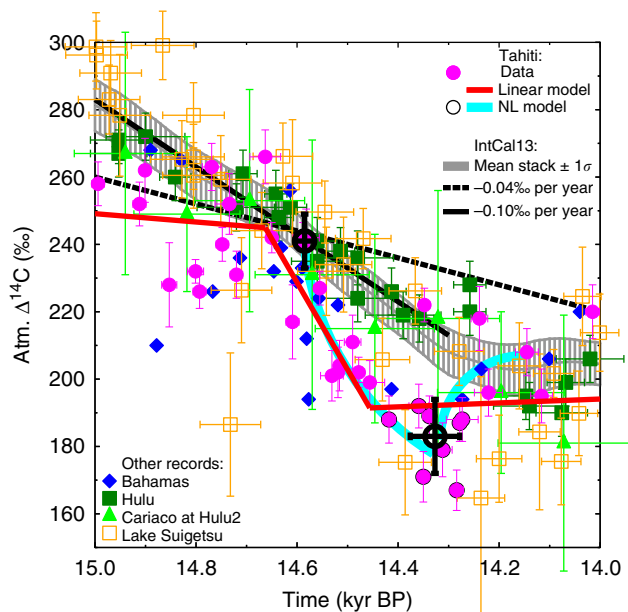
Although this analysis of CH_4 and CO_2 changes gives some first ideas on the potential cause of the abrupt CO_2 rise around the onset of the B/A, its ultimate source was so far not identified. The $\delta^{13}C$ signature of terrestrial or marine carbon sources are different and might allow some source detection. However, the data uncertainty and density of the atmospheric $\delta^{13}CO_2$ record did so far not allow such an identification[6]. A high-resolution U/Th-dated time series of atmospheric $\Delta^{14}C$ derived from Tahiti corals[7] over that event offers now some new and independent insights on the exact timing and magnitude of the carbon release event and brings some suggestions on its potential origin.

Here we show that the synchronous change in atmospheric $\Delta^{14}C$ and CO_2 derived from the Tahiti and EDC data sets at the onset of the B/A can be explained by the same process and suggest permafrost thawing being this process. We finally examine the climate impact of the GHG changes around 14.6 kyr BP using a state-of-the-art-coupled Earth system model. Special focus of these investigations is the imprint of the GHG changes on the Antarctic temperature signature and the relevance of these changes for the interpretation of bipolar climate linkages during abrupt climate changes[8].

Results

Atmospheric $\Delta^{14}C$ and ice core CO_2. The new coral-based atmospheric $\Delta^{14}C$ record from Tahiti[7] shows a prominent decline around 14.6 kyr BP, an anomaly not visible in the IntCal13 $\Delta^{14}C$ stack[9] (Fig. 2). For comparison, we briefly discuss specific details related to IntCal13 and what other ^{14}C archives record at that point in time: After 13.9 kyr BP IntCal13 is based on tree rings with very little variability. For older samples, however, the various archives differ by more than the measurement errors. A $\Delta^{14}C$ anomaly similar to the Tahiti data can be seen in speleothems from Bahamas[10] (Fig. 2). The anomaly is not seen in speleothems from the Hulu Cave[11] or in the marine sediments from Cariaco[12] (Fig. 2). The Cariaco record bears some problems—therefore, a part of it has been excluded by the IntCal13 group specifically during the Heinrich 1 event, that is, just before the B/A[9]. Necessary corrections of speleothem ^{14}C data for its dead carbon fraction (DCF) introduce large uncertainties to atmospheric $\Delta^{14}C$ based on them[9]. Furthermore, the DCF is not constant but depends itself on climate[13] making the speleothems an archive difficult to interpret, especially during rapid climate changes. The signal might thus potentially be smoothed out in Hulu, as the DCF acts as a low-pass filter. The best recorder of atmospheric $\Delta^{14}C$ available up to now might be the terrestrial plant material derived from Lake Suigetsu[14]. Here no corrections for the reservoir effect or for DCF are necessary. The Lake Suigetsu data, however, are rather scattered over the time interval of interest, show a steeper decline in $\Delta^{14}C$ than IntCal13, but neither strongly support IntCal13 nor Tahiti (Fig. 2). Altogether, the evidences from $\Delta^{14}C$ data are mixed and further data are necessary for a conclusive interpretation.

The coral-based $\Delta^{14}C$ record from Tahiti is corrected for a reservoir age[15] of constantly 300 ^{14}C years[7] to be interpreted as atmospheric $\Delta^{14}C$. In principle, the reservoir age might change over time, mainly due to ocean circulation changes. However, simulations with three different models[16–18] suggest that the

Figure 1 | Relevant ice core and $\Delta^{14}C$ data during Termination I.
Atmospheric $\Delta^{14}C$ based on Tahiti corals (magenta circles, mean $\pm 1\sigma$)[7] or IntCal13 (grey area, $\pm 1\sigma$ uncertainty band around the mean)[9], the latter including linear trends with $-0.04‰$ per year or $-0.10‰$ per year; CO_2 from EDC (blue filled circles)[1,22,68]; CH_4 from EDC (blue)[22] and Greenland (red)[69]; WAIS Divide (WD) $\delta^{18}O$ (original (blue) and 100 years running mean (yellow))[54]; stack of calculated temperature change[3] ΔT_{ANT} from the five East Antarctic ice cores EDC, EPICA DML, Vostok, Dome Fuji and Talos Dome (original (black) and 100 years running mean (orange)); NGRIP[70] $\delta^{18}O$. All Greenland records on GICC05 (ref. 23), all EDC records on AICC2012 chronology[4], WD and ΔT_{ANT} on their own independent chronology.

Figure 2 | Data analysis of atmospheric Δ^{14}C around 14.6 kyr BP.
Atmospheric Δ^{14}C based on Tahiti corals[7] (magenta circles) and IntCal13 (grey line, $\pm 1\sigma$ uncertainty band around the mean)[9] are analysed for trends and compared with various other archives (speleothems from Bahamas[10] (blue diamonds), Hulu Cave[11] (dark green squares), marine sediments in Cariaco[12] (light green triangles) plotted on revised Hulu2 age model[9], Lake Suigetsu[14] (orange open squares)). All individual data points are plotted with $\pm 1\sigma$ in both age and Δ^{14}C. IntCal13 was approximated by a linear trend with either -0.04‰ per year (black solid line) or -0.10‰ per year (black dashed line). Tahiti data were analysed for break points with two different models (see Methods). For the linear model (red lines), a statistical package was used. For the non-linear (NL) model (cyan lines), two data points at beginning of the Tahiti data Δ^{14}C anomaly from the IntCal13 data and the eight points around the local minimum (black open circles) were averaged, plotted with $\pm 1\sigma$ in both age and Δ^{14}C (bold large black open circles) and further analysed. The anomaly in the Tahiti Δ^{14}C data following the linear model is $\Delta(\Delta^{14}C) = -54 \pm 8$‰ in $\Delta(age) = 207 \pm 95$ years and following the NL model: $\Delta(\Delta^{14}C) = -58 \pm 14$‰ in $\Delta(age) = 258 \pm 53$ years.

reservoir age is relatively stable in the central Pacific around Tahiti for various ocean circulation changes (see Supplementary Note 1 for details). We therefore assume that reservoir ages did not change over the last 15 kyr in the central low-latitude Pacific and the Δ^{14}C signal based on Tahiti corals is not based on local effects but indeed a recorder of atmospheric Δ^{14}C changes.

We date the start of this Δ^{14}C decline seen in the Tahiti data with two different approaches (Fig. 2, methods) with a 1σ uncertainty of less than a century to 14.6 kyr BP and calculate a Δ^{14}C decline of ~ 55‰ within 200 to 250 years. Having already excluded changes in reservoir age, we are left with either a modified carbon cycle or reduced ^{14}C production rates as potential process explaining the Tahiti Δ^{14}C data. On the basis of available ^{10}Be, data changes in ^{14}C production rates cannot convincingly explain the Δ^{14}C data (Supplementary Fig. 1, Supplementary Note 1). All our tests therefore indicate that the Tahiti Δ^{14}C drop at 14.6 kyr BP is caused by carbon cycle changes. This is our working hypothesis on which all else is based on, but note that its failure cannot entirely be ruled out.

Carbon cycle changes responsible for the Δ^{14}C anomaly would also leave their imprints on atmospheric CO_2. We can therefore use the absolute U/Th-dated Δ^{14}C from the Tahiti corals as an independent time constraint on the atmospheric CO_2 rise. This is

a novel new approach to synchronize atmospheric Δ^{14}C and atmospheric CO_2, because ice cores archive only a smoothed version of the atmospheric concentrations making an exact dating of the abrupt change in atmospheric CO_2 very difficult[6]. Furthermore, firnification and gas enclosure are still not completely understood[19], and the age difference between ice matrix and embedded gases complicates gas chronologies[3]. On the most recent chronology[4], AICC2012, CO_2 measured in situ in the EDC ice core rises by 10 p.p.m.v. between 14.81 and 14.68 kyr BP. This is more than a century faster when compared with previous chronologies[3] (Figs 3a and 4b), but might in detail be revised even further once the most recent understanding of firnification is applied[20]. Atmospheric changes in CO_2 need to have happened even more abruptly than what is recorded in ice cores[6].

Here we use the Tahiti Δ^{14}C as an independent age constraint for the start of the carbon cycle changes (14.6 kyr BP). Recently, others[21] have shown that the rise in atmospheric CH_4 and in temperature in Greenland are near synchronous (5 ± 25 years) at the onset of the B/A warming. From previous GHG records measured at the EDC ice core[22], it is known that CO_2 and CH_4 also rise synchronously at 14.6 kyr BP. Combining this information, we have to conclude that the rise in atmospheric CO_2 and CH_4 together with the rapid warming of the northern hemisphere (NH) happened at the same time, and started at 14.6 kyr BP. This is only 35 years later than the suggested age of the onset of the B/A (14.635 ± 0.186 kyr BP, $\pm 1\sigma$) in the annual-layer counted NGRIP ice core[23,24], well within the dating uncertainty of GICC05 (Fig. 5).

Carbon cycle simulations. A release of 125 Pg of C into the atmosphere within a time window of 50 to 200 years was proposed before[6] to explain the rise of 10 p.p.m.v. in CO_2 measured in EDC. The true atmospheric CO_2 then shows an overshoot whose peak amplitude mainly depends on the length of the assumed release time (Supplementary Fig. 2). Furthermore, low-resolution CO_2 time series from other ice cores with amplitudes of 17, 15 and 19 p.p.m.v. in Byrd, Taylor and Siple Dome, respectively[25–28] (Fig. 3a), indicate that the true atmospheric signal had a larger amplitude than what was measured in situ in EDC[6].

In our previous analysis, we also investigated atmospheric $\delta^{13}CO_2$, from which the potential source of the released carbon might have been identified. The new compilation of ice core $\delta^{13}CO_2$ data published in the mean time[1] offers a new look on the information contained in that record. This $\delta^{13}CO_2$ compilation is now based on data from EDC, EPICA DML and Talos Dome. In our time window of interest (15–14 kyr BP), however, only data from EDC were obtained with some new data points adding to the previous record. This revised $\delta^{13}CO_2$ record shows a drop by 0.1‰ around 14.7 kyr BP followed by a subsequent rise by ~ 0.2‰ at 14.4 kyr BP (Fig. 3b). Distinguishing terrestrial from marine carbon sources for our carbon release leads in our best-guess scenarios (see below how that was chosen) to either a drop in $\delta^{13}CO_2$ of 0.4‰ or less than 0.1‰ in the true atmospheric signal, respectively, but only to -0.15‰ and less than -0.05‰ in a time series that would be recorded in EDC (Fig. 3b). Both marine- and terrestrial-based $\delta^{13}CO_2$ simulations fall within the uncertainties of the measurements before 14.6 kyr BP. The small rise in $\delta^{13}CO_2$ after 14.4 kyr BP, however, indicates that directly after the onset of the B/A other processes released less δ^{13}C-depleted carbon to the atmosphere, for example, CO_2 outgassing from warm oceanic surface waters. On the basis of the data uncertainty of $\delta^{13}CO_2$ in EDC, it is still impossible to clearly identify if the released carbon was of marine or terrestrial origin.
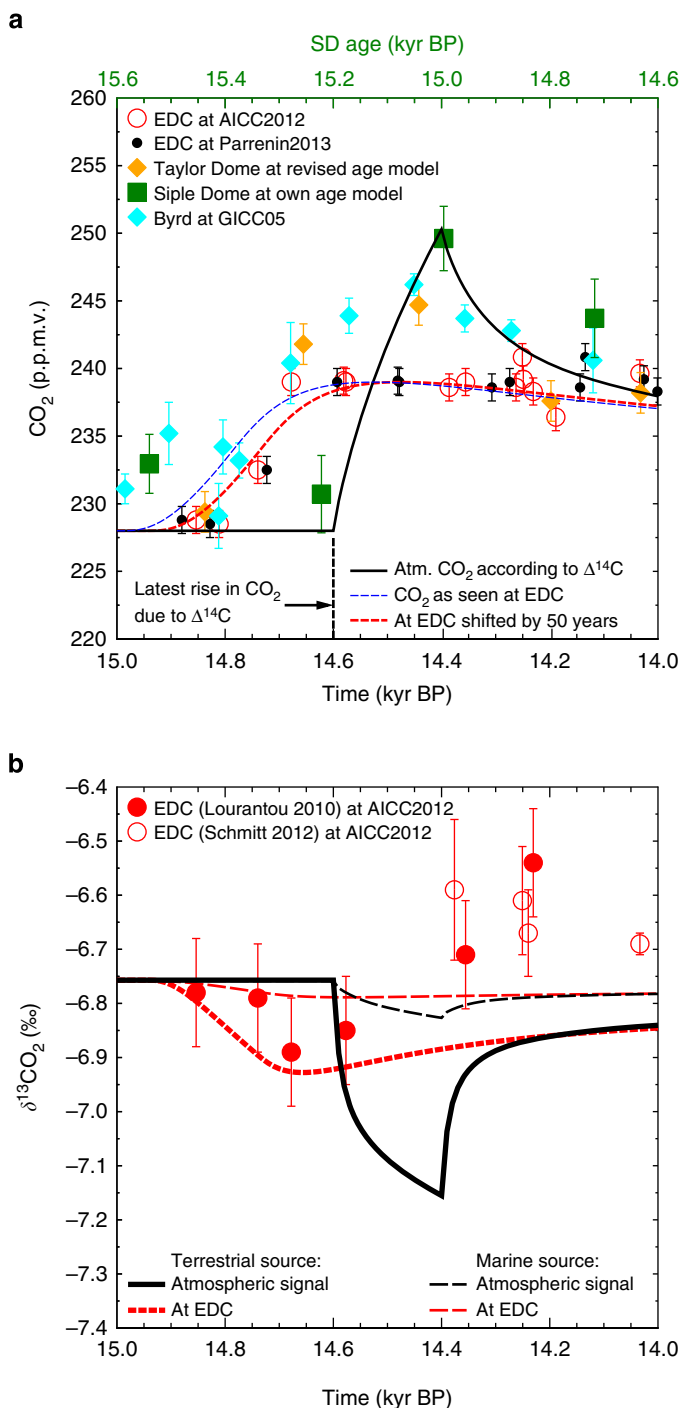
Figure 3 | Ice core and simulated true atmospheric CO_2 and $\delta^{13}CO_2$.
(**a**) Ice core CO_2 data ($\pm 1\sigma$) from EDC[1,22,68] on two different chronologies[3,4] AICC2012 and Parrenin2013, Taylor Dome on revised age model[26,27], Siple Dome on own age model (top x axis)[27], Byrd on age model GICC05 (refs 25,28). Simulated true atmospheric CO_2 in our best-guess scenario according to ^{14}C data (black bold line), filtered to a signal that might be recorded in EDC (blue dashed line), shifted by 50 years to meet the EDC data (dashed red line). (**b**) Ice core $\delta^{13}CO_2$ data ($\pm 1\sigma$) from EDC[1,68], simulated true atmospheric $\delta^{13}CO_2$ of our best-guess scenario and how it would have been recorded in EDC for either terrestrial or marine origin of the released carbon, implying a $\delta^{13}C$ signature of -22.5 or -8.5‰, respectively.

Using the same carbon cycle model[6], we repeat simulations of carbon release with special focus on ^{14}C. The model dynamic with respect to ^{14}C was extensively evaluated

(Supplementary Note 2). We assume a depletion in ^{14}C of the released carbon with respect to the atmosphere ($\Delta(\Delta^{14}C)$) between -50 and $-1,250\text{‰}$. This range in the ^{14}C anomalies covers carbon sources from the mean terrestrial biosphere potentially released by shelf flooding[6] (-50‰), suggested signatures of old carbon of Pacific intermediate waters as measured off Baja California[29] (-400‰) and Galapagos[30] (-700‰) to a maximum effect of ^{14}C-free carbon ($-1,250\text{‰}$). The Shelf Flooding Hypothesis is explained in detail in the next section, and some more details on our assumptions on ^{14}C are found in the methods.

The highest-simulated anomalies in atmospheric $\Delta^{14}C$ are obtained for short release times reaching -100‰ for 50 years and the largest $\Delta(\Delta^{14}C)$ of $-1,250\text{‰}$ (Fig. 4c). The amplitudes drastically decline with longer release time towards less than -35‰. $\Delta^{14}C$ anomalies are significantly smaller if $\Delta(\Delta^{14}C)$ was -700‰ or less (Fig. 4c). Because of the distinct dynamics of the $\Delta^{14}C$ data, release times shorter than ~110 years are at odds with the Tahiti ^{14}C reconstruction. Simulated anomalies in atmospheric carbon records are nearly identical for Atlantic meridional overturning circulation (AMOC) in the strong or weak mode (Methods, Fig. 4c, Supplementary Fig. 3). Combining the information from both the ice core data and our analysis of the Tahiti $\Delta^{14}C$ data leads to a range of scenarios with carbon release times between ~110 and 200 years in which model results and data agree (Fig. 4c). The range of possible scenarios fulfilling the data constraints also includes some with $\Delta(\Delta^{14}C)$ between -700 and $-1,250\text{‰}$, and so we cannot entirely exclude the possibility that the released carbon still contains some ^{14}C. From these possible scenarios, we selected the one with the longest release time of 200 years to be our best-guess scenario, because short release times lead to higher amplitudes in atmospheric CO_2, which are not supported by other ice core data. This scenario pinpoints to a $\Delta(\Delta^{14}C)$ of $-1,250\text{‰}$ resulting in peak amplitudes of -42‰ in atmospheric $\Delta^{14}C$ (Fig. 4c) and of $+22$ p.p.m.v. in atmospheric CO_2 (Fig. 4d). The depletion in ^{14}C necessary for the model output to agree with the data implies that the shelf flooding hypothesis connected with meltwater pulse 1A (MWP-1A)[6,31] seems at a first glance to be in disagreement with the Tahiti-based atmospheric $\Delta^{14}C$ reconstructions (Fig. 4c). We discuss details on a potential contribution connected with MWP-1A further below. The release of deep ocean carbon, although so far not suggested to play a role during this rapid CO_2 rise, might only potentially be responsible here, if water masses are detected, which are even more depleted in ^{14}C than what is known until now[29,30].

The Tahiti $\Delta^{14}C$ data show an excursion from the long-term declining trend of IntCal13 (ref. 9) (Figs 1 and 4a). Depending on the time window of interest, IntCal13 might be approximated by a linear fit with a slope of -0.04‰ per year (the whole Mystery Interval, 19–14 kyr BP) or -0.10‰ per year (15.0–14.3 kyr BP), respectively. These long-term changes are probably caused by a mixture of changes in ^{14}C production rate and the carbon cycle[32]. While we are able to force our model with changing ^{14}C production rates (Supplementary Fig. 4), all relevant processes in the carbon cycle are not yet identified. We therefore compare the $\Delta^{14}C$ data with our original simulation results based on constant ^{14}C production rate, but also with some results that are corrected for the trend seen in IntCal13. If corrected accordingly, our best-guess scenario finally meets the amplitude in the Tahiti $\Delta^{14}C$ data (Fig. 4a,c).

Evidence for permafrost thawing. The synchronicity of the NH warming and the carbon cycle change together with our suggested hypothesis for the injection of nearly ^{14}C-free carbon into the atmosphere make permafrost thawing and a subsequent release of
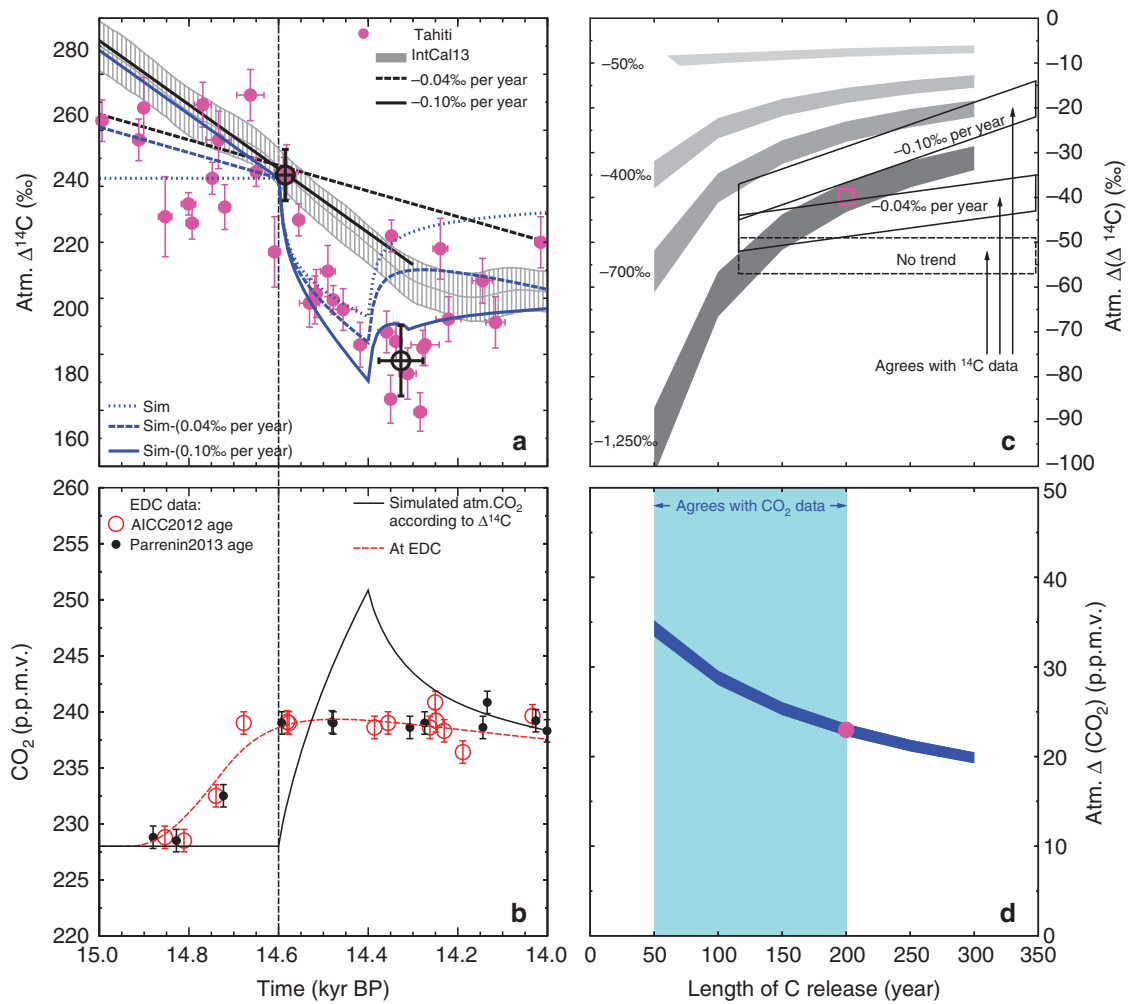
Figure 4 | Main carbon cycle simulation results. The transient simulation results (left) showing the impact of a carbon release event on true atmospheric $\Delta^{14}C$ and CO_2 obtained with the carbon cycle model BICYCLE for the best-guess scenario are compared with the data. In sensitivity studies (right), the length of the release event and the radiocarbon signature $\Delta(\Delta^{14}C)$ of the released carbon are constrained by the data. (**a**) Atmospheric $\Delta^{14}C$ data from Tahiti corals[7] (magenta, mean $\pm 1\sigma$ in both age and $\Delta^{14}C$) and IntCal13 (ref. 9) (grey band, mean $\pm 1\sigma$) data. Black bold circles denote start and stop ($\pm 1\sigma$) of carbon release in the non-linear model of the Tahiti data interpretation. The vertical black dashed line marks the estimated started of carbon release at 14.6 kyr BP based on a combination of different explanations. Best-guess simulation results of atmospheric $\Delta^{14}C$ (blue) superimposed by a linear trend of either $-0.04‰$ per year (long dashed line) or $-0.10‰$ per year (solid line) (short dashed: no trend superimposed). (**b**) Atmospheric CO_2. EDC ice core CO_2 data (mean $\pm 1\sigma$) on two different chronologies[3,4] AICC2012 and Parrenin2013. Simulated true atmospheric CO_2 rise (black bold line), and how the signal might be recorded in EDC (dashed red line) after filtering for gas enclosure and shifted by 50 years to meet the data. (**c**) Simulated peak height in atmospheric $\Delta^{14}C$ (grey areas) as function of length of carbon release and of the $\Delta^{14}C$ depletion. (**d**) Simulated peak height in atmospheric CO_2 (dark blue area) as function of length of carbon release. In **c,d**, simulations result with the AMOC in either a weak or a strong mode are combined spanning a range of results. Magenta square and circle in **c,d** mark results of our best-guess scenario for $\Delta^{14}C$ and CO_2, respectively. We colour coded the areas in the parameter space where simulation results agree with the EDC CO_2 data (**d**, light blue) and with the interpretation of the Tahiti $\Delta^{14}C$ data (**c**, black boxes). The latter are modified for background linear trends already contained in IntCal13 based on other processes.

old soil carbon a prominent candidate to explain the atmospheric carbon records. The age of carbon stored in permafrost soils during glacial times is unknown. Throughout the last glacial cycle Greenland and the whole NH was perturbed by the rapid warming of Dansgaard/Oeschger (D/O) events[33]. However, during the last 80 kyr, only D/O event 12 around 47 kyr BP reached in a temperature reconstruction for the site of the NGRIP ice core in Greenland similar high temperatures as the B/A (Fig. 6b). In this NGRIP, temperature time series D/O event 2 around 23 kyr BP was rather weak and short, but D/O event 3 at 28 kyr BP reached with $-36\,°C$ nearly the temperature of $-33\,°C$ of the B/A[33] (Fig. 6b). We assume that most of the NH follow this temporal changes in temperature observed for Greenland, although with warmer temperatures closer to the

freezing point further south. It might then be that large areas of the NH were permanently frozen after D/O event 3, thus about 13 kyr before thawing induced by the onset of the B/A. The $\Delta^{14}C$ of that permafrost carbon would be depleted by $-900‰$ with respect to atmospheric $\Delta^{14}C$ during release around 14.6 kyr BP (Fig. 6a). However, soil carbon might age significantly in high latitudes before freezing, for example, present day North American peatlands are up to 17-kyr old[34]. Such soil ageing reduces ^{14}C even further. If the precursor material of the permafrost soil carbon was photosynthetically produced during D/O event 12 around 47 kyr BP (the next preceding period comparable in temperature to the B/A, Fig. 6b), it would be essentially free of ^{14}C and depleted with respect to atmospheric $\Delta^{14}C$ by nearly $-1,250‰$ (Fig. 6a). Permafrost thawing would
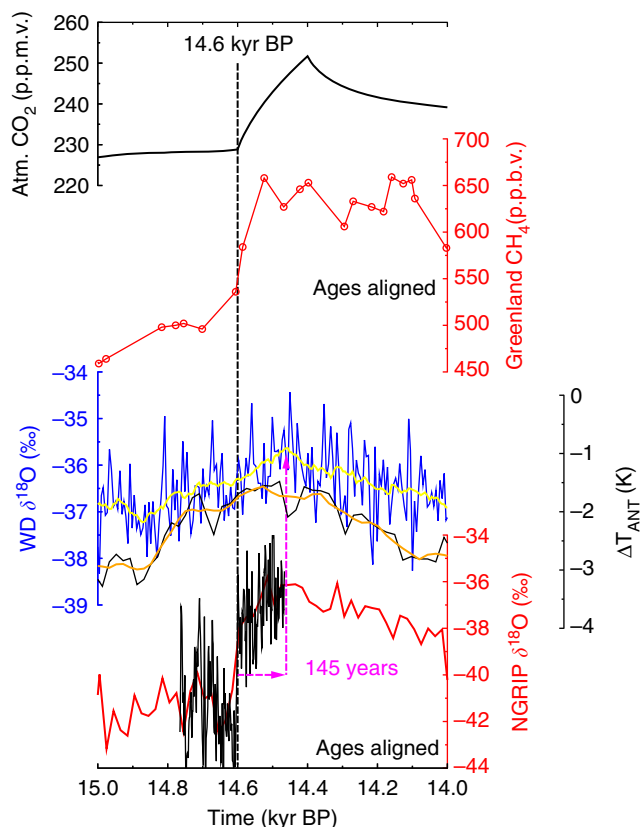
Figure 5 | Implication on the timing of abrupt climate change as obtained in various ice core records from Greenland and Antarctica. Our results suggest that anomalies in Tahiti $\Delta^{14}C$ and true atmospheric CO_2 are caused by the same process. This information is used here as an independent age constraint. The onset of the abrupt rise in atmospheric CO_2 (black bold, this study) is thus tied to 14.6 kyr BP. From previous ice core analysis[22], it is known that the rise in CO_2 and CH_4 (red circles, Greenland composite[69]) occur synchronously here. A new study[21] on the NEEM ice core tied the CH_4 rise to be near synchronous to Greenland temperature rise. This synchronicity of the start of the abrupt changes in atmospheric CO_2, CH_4 and Greenland temperature tied to 14.6 kyr BP led to the age alignments in CH_4 and NGRIP $\delta^{18}O$ (high[24] (black thin line) and low[70] (red line) resolution). We furthermore show some Antarctic climate records on their own independent chronologies to illustrate the temporal north–south offsets. WD[54] $\delta^{18}O$, original (blue) and 100 years running mean (yellow) and stack[3] of temperature change from five ice cores in East Antarctica, ΔT_{ANT}, original (black) and 100 years running mean (orange).

then contain a depletion in $\Delta^{14}C$, which is more negative than for all other suggested processes[6,29,30]. An alternative scenario based on the destabilization of gas hydrates, which also contain ^{14}C-free carbon, can be rejected based on CH_4 isotopes[35–37].

For the present day, a rise in global mean temperature by 5 K, which because of polar amplification might represent a northern high latitude warming of 10 K, was proposed to lead to the release of more than 130 Pg of soil carbon from permafrost thawing within 200 years[38]. Greenland ice core data[33] and simulations[39] suggest that temperatures in the B/A rose by 10–15 K to near preindustrial levels in central Greenland and throughout most of the NH land areas. A large inert terrestrial carbon pool consisting of permafrost soils containing 700 Pg more C at the Last Glacial Maximum (LGM) than at present day has been proposed[40], which needs to release its excess carbon during deglaciation. The areal extent of continuous permafrost at LGM (Fig. 7) was calculated from models[41] in PMIP3 to
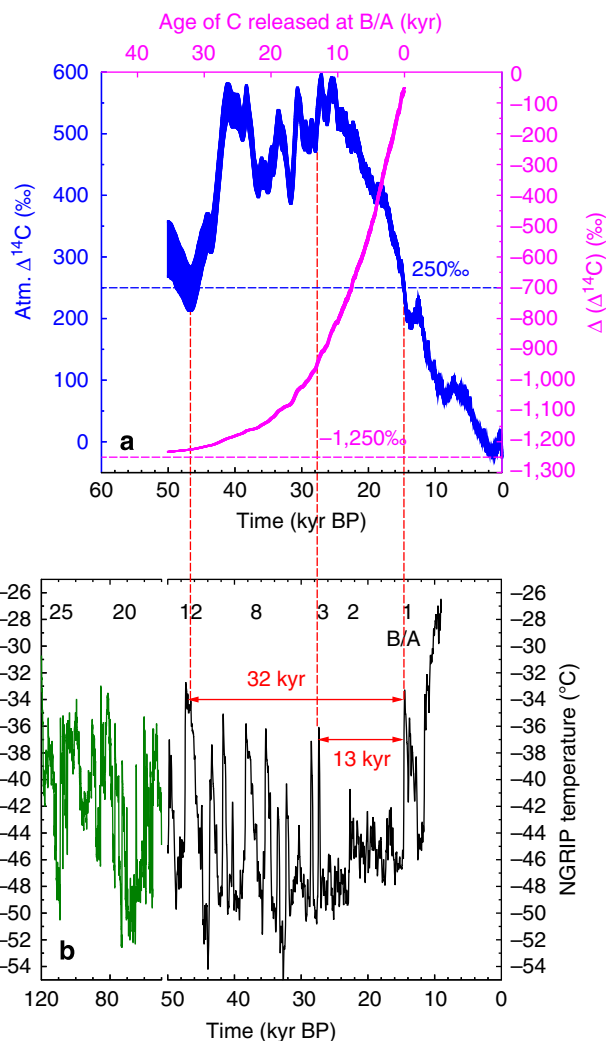
Figure 6 | Radiocarbon depletion of soil carbon of different age and high northern latitude climate change. (a) Atmospheric $\Delta^{14}C$ based on IntCal13 (ref. 9) over the last 50 kyr (blue, left y axis, mean $\pm 1\sigma$). Calculated radiocarbon depletion resulting in $\Delta(\Delta^{14}C)$ (mean $\pm 1\sigma$) of soil carbon released during the B/A as a function of its age (magenta, right y axis, upper x axis) and of atmospheric $\Delta^{14}C$ during time of production. (b) NGRIP temperature reconstruction[33] from 120 to 10 kyr BP. The time series is plotted in two different colours because of the break in the x axis scale at 50 kyr BP. Numbers label selected D/O events. Red labelled arrows highlight the time which past since NGRIP was similar as warm as during the B/A (32 kyr since D/O event 12) and since the previous significant warming before the B/A (13 kyr since D/O 3).

26×10^{12} m^{-2}, agrees with reconstructions[42], and is twice as large as for preindustrial times[41].

Previously, methane isotopes[36] suggested that a rise in boreal wetland CH_4 emissions by $+32$ Tg CH_4 per year would explain the CH_4 rise into the B/A. These findings[36] have been challenged by new methane isotope data[37], but so far no revised CH_4 emissions from boreal wetlands have been calculated for the B/A. An alternative interpretation[5] of the CH_4 cycle based on its interhemispheric gradient suggests that the rise in CH_4 by 150 p.p.b.v. at the onset of the B/A was largely driven by the increase in CH_4 emissions from both tropical ($+35$ Tg CH_4 per year) and boreal ($+15$ Tg CH_4 per year) wetlands. The CH_4 change at the onset of the B/A is thus clearly dominated by tropical wetlands and its conclusive interpretation is beyond the scope of this study. However, the rise in CH_4 emissions from
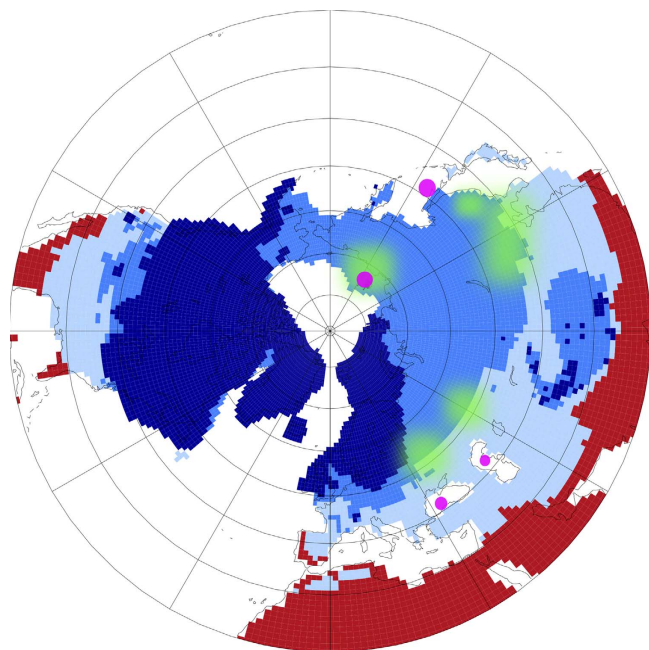
Figure 7 | PMIP3 simulation results on the LGM permafrost extend.
Results[41] show a polar projection of the NH from 20 °N northwards, are based on soil temperature and distinguish land with ice (dark blue), permafrost (blue), seasonal frozen (light blue) and not frozen (red). Present day coastlines are sketched in thin black lines. Magenta points mark potential core sites (Siberian Shelf, Black Sea, Caspian Sea, Sea of Okhotsk) from which future ^{14}C measurements on terrigenous material might verify the age of permafrost possible thawed around 14.6 kyr BP (suggested green areas).

boreal wetlands is nearly identical to the rise in emissions of up to + 14 Tg CH_4 per year projected from deep permafrost thawing of the next century[43]. If this rise in the boreal CH_4 flux is integrated over the 200-year time window of our carbon release scenario, a total of 3.0 Pg of CH_4 (or 2.25 Pg C in the form of CH_4) might have been released. This is ~2% of our total estimated carbon emissions of 125 Pg C, and in line with an expert assessment on the future vulnerability of permafrost[44] estimating that 2–3% of carbon released by thawing might enter to the atmosphere in the form of CH_4. Although the contribution from boreal wetlands to the CH_4 rises at the onset of the B/A is small, the nearly ^{14}C-free signature connected with our proposed permafrost thawing might be tested by ^{14}C measurements on CH_4 derived from ice cores[45].

So far, we suggested that NH permafrost is the responsible source of the released carbon. In the following, we hypothesize which region might have been affected in detail by permafrost thawing and how this can be tested in future studies. The PMIP3-based map on the LGM permafrost extent clearly indicates that the largest areas with continuous permafrost are found in northern Siberia (Fig. 7). Thus, evidences of permafrost thawing connected to the NH warming should be expected in outflow originated from the southern edge of the LGM permafrost area (around 40–50°N), which thawed first. A lot of these areas are drained via the Amur river into the Sea of Okhotsk and into coastal seas towards the south (Caspian and Black Sea). Indeed, a combination of terrestrial biomarkers that clearly indicate the thawing of permafrost was found at the onset of the B/A in a sediment core drilled in the Black Sea that records the drainage from the Fennoscandian Ice Sheet[46]. Here variations in the normalized concentrations of different long-chain molecules provide information on changes in the abundance of peat-forming plants. Such data are useful indicators for the variation of

permafrost thawing and of wetland extension as well as for fluvial periglacial soil erosion in its drainage basin. In details, this study[46] provides evidence that the permafrost melting was very intense only during the initial part of the Bølling corresponding indeed to the sharp NH warming.

The map (Fig. 7) also shows that a large fraction of the Siberian shelf in the Arctic Ocean was during the LGM covered by permafrost. It might thus be possible that MWP-1A, which was recorded as a rise in sea level at Tahiti[31] from about − 105 to − 85 m between 14.65 and 14.31 kyr BP might be partially responsible for the carbon release as initially suggested[6]. The flooding of continental shelves was also proposed to contribute to the CH_4 rise during deglaciation and during D/O events[47]. In our earlier study[6], we proposed that mainly the flooding of the Sunda Shelf followed by tropical rain forest decay might have been responsible for the carbon release. This shelf flooding scenario was here addressed with a $\Delta(\Delta^{14}C)$ of − 50‰ for mean terrestrial carbon, which failed to meet the $\Delta^{14}C$ data. In our earlier study[6], we also discussed that the existing time series of sea level change suggest that before MWP-1A the shelves were last flooded around 30 kyr BP, 15 kyr earlier, leaving ample time for ^{14}C in permafrost carbon on the shelf to decay and to produce a $\Delta(\Delta^{14}C)$ in the released carbon of down to − 900‰ (Fig. 6). Most recent sediment data[48] on iceberg discharge in Antarctica during Termination I found a significant Antarctic contribution to MWP-1A. Fingerprint analysis[49] of different water sources for MWP-1A indicate that sea level would rise locally by up to 50% above global average on the Siberian Shelf for freshwater released in Antarctica. When considering the source-depending overprint[49], we calculate, based on the present day bathymetry[50], a maximum areal extent of $0.4 \times 10^{12} \, m^{-2}$ of the Siberian Shelf, which might have been flooded by MWP-1A. This is the same order of magnitude as the present day Siberian Yedoma deposit extent[51] from which an organic carbon content of 30–140 Pg C has been proposed[51]. Coastal erosion and sub-sea permafrost release in Arctic Siberia are also observed for modern times[52] with a $\Delta^{14}C$ signature of the released organic carbon as low as − 800‰. Modern organic carbon content in Eurasian Arctic[53] river runoff have $\Delta^{14}C$ ages of up to 10 kyr. All these modern data indicate that old carbon in permafrost exists nowadays, and potentially was more abundant and older during glacial times.

In which region the thawing of permafrost finally happened might be verified by future ^{14}C measurements on terrigenous organic material that are retrieved from marine sediments in the suggested coastal seas. It will then be possible to finally attribute the size of the released carbon to either a pure thermodynamically thawing at the southern edge of the permafrost area or to a contribution from flooding the Siberian Shelf during MWP-1A.

Discussion

The rapid CO_2 rise at the onset of the B/A is contained with different amplitude in various ice cores (Fig. 3a). However, the uncertainty in the proposed age distribution of the CO_2 in EDC is still large[6] (Supplementary Fig. 2c) and the assumed carbon release history and the applied carbon cycle model influence the amplitude of the proposed true atmospheric CO_2 rise. Future CO_2 measurement from the WD ice core[54] might refine some of these aspects. The WD ice core has an order of magnitude higher present day accumulation rate than EDC (20 versus ~3 g cm^{-2} per year), thus offers temporally higher resolved gas records. A potential WD CO_2 record still needs to be corrected for the smoothing during firn enclosure, although this effect will be a lot smaller than for EDC. Only by considering the 20% uncertainty in the mean exchange time of CO_2 before enclosure in EDC

(Supplementary Fig. 2c) would result in a CO_2 release and an amplitude in the true atmospheric CO_2 rise, which are also 20% smaller than in our best-guess scenario, for example, releasing 100 instead of 125 Pg C leading to a true atmospheric CO_2 amplitude of 18 instead of 22 p.p.m.v. (Supplementary Fig. 2d). Results are then still within the range given by the EDC CO_2 data (Supplementary Fig. 2d). Furthermore, we calculate that a 33% reduction in the proposed carbon released to the atmosphere (85 instead of 125 Pg C) still fulfils the data constrains given by the Tahiti $\Delta^{14}C$ record.

Other rapid CO_2 rises are detected in EDC at the end of the Younger Dryas and in Marine Isotope Stage (MIS) 3 in other ice cores[55]. Whether they are also caused by permafrost thawing is not investigated here. However, these other rapid CO_2 jumps are not always connected to a warming of the NH. Furthermore, the missing of ^{14}C-depleted CH_4 during the CO_2 rise at the end of the Younger Dryas around 12 kyr BP[45] suggests that other processes are responsible. Moreover, our suggested old soil carbon release during permafrost thawing at 14.6 kyr BP, requires that the same carbon sources were not tapped during other events within Termination I. Again, ^{14}C measurements on terrigenous material might clarify how old the carbon released from permafrost was or if earlier CO_2 rises might already have consumed the old, ^{14}C-depleted carbon.

Our study suggests that for Termination I, abrupt warming in the NH might lead to massive permafrost thawing, activating a long-term immobile carbon reservoir. The abruptly released carbon then amplified the initial warming as a positive feedback. Our best-guess scenario generates together with the rise in the other two important GHG CH_4 and N_2O a radiative forcing[6] of $\sim 0.7\,W\,m^{-2}$. It is important to quantify the feedback of this GHG forcing on climate to better understand the impact of the abrupt GHG changes during the last deglaciation. Since the abrupt GHG changes are contemporaneous with the onset of the B/A (in the North) and the beginning of the ACR (in the South), the sequence of the associated bipolar climate linkages are of particular interest.

Therefore, we have conducted transient simulations with our best-guess reconstruction of atmospheric GHG changes during the beginning of the B/A and the ACR, using the Earth System Model COSMOS[16,56] in a coupled atmosphere-ocean configuration as outlined in detail in the Supplementary Note 3. To evaluate the global impacts of the GHG changes it is instructive to analyse Antarctic temperature changes, since temperature changes obtained from Antarctic ice cores have been shown to reflect global scale climate changes associated with CO_2 variations particularly well[57]. On the basis of our climate model investigations, we find that the abrupt rise in GHG concentrations provides an important impact on the Antarctic temperature signature associated with an abrupt AMOC strengthening at the end of Heinrich Stadial 1 (Supplementary Fig. 5). This highlights a potential contribution of abrupt GHG changes on the bipolar climate signature during deglaciation. In this sense, the abrupt GHG changes would be a factor that would offset the timing of the temperature maximum leading into the ACR, compared to the onset of the B/A. As layed out in detail in the climate feedback section of the Supplementary Note 3, also smaller GHG spikes bear the potential to have a substantial effect on the Antarctic temperature response when compared with impacts caused by AMOC changes.

So far a synthetic record of Greenland temperature changes[8] seems to indicate that rapid climate changes in the north might indeed have been a universal feature of deglaciations during the last 800 kyr. Hence, similar to the last deglaciation, abrupt permafrost thawing might have also occurred regularly during earlier terminations, although further studies are necessary here.

Termination II also contains[58] an abrupt rise in CO_2, synchronous to a rise in CH_4. A massive drop in atmospheric $\delta^{13}CO_2$ accompanying this event[58] is consistent with the release of $\delta^{13}C$-depleted CO_2 that might indicate a terrestrial source. However, new $\delta^{13}CO_2$ data[59] did not confirm this negative $\delta^{13}CO_2$ anomaly and the revised data give no indication on the source of this CO_2 rise. A synchronous change in deuterium excess[60], a proxy for moisture source shifts, has been used to suggest that abrupt shifts in southern westerlies might be connected with the CO_2 rise[61], but a compelling explanation remains elusive and further testing of permafrost thawing as a possible alternative interpretation is needed.

In conclusion, we here suggest that the processes responsible for the abrupt CO_2 rise at the onset of the B/A is also the underlying cause for the drop seen in atmospheric $\Delta^{14}C$ based on Tahiti corals. This connection offers a U/Th-dated tie point for the start of the massive release of carbon at 14.6 kyr BP. Using a carbon cycle box model, and assuming the release of 125 Pg of nearly ^{14}C-free carbon, we are able to explain observed anomalies in atmospheric CO_2 and $\Delta^{14}C$. On the basis of the ^{14}C signature of the released carbon and the synchronicity to the warming of the NH, we suggest that the thawing of permafrost was this responsible process. A potential contribution from MWP-1A flooding the Siberian Shelf, which might have contained a large amount of permafrost, is also possible. Future ^{14}C measurements on terrigenous material might further constrain the source region. Our interpretation not only provides conceptual insights into the source of the excursions in the atmospheric carbon records around 14.6 kyr BP, but also offers an alternative to explanations[62,63] for the interhemispheric timing of the B/A and the ACR as found in ice cores from both hemispheres. Taken together, our findings highlight a potential climate feedback that might be obtained from abrupt CO_2 release during deglaciation. This analysis furthermore indicates that the proposed carbon cycle feedback from an anthropogenic driven permafrost thawing in the near future[38,43,44,64] may already have happened in a similar way in the past.

Methods

Analysis of the $\Delta^{14}C$ data. For analysis of the drop in the atmospheric $\Delta^{14}C$ data based on Tahiti corals, we used two different approaches (Fig. 2). First, we used a linear statistical model Breakfit[65], which calculates the break points in time series. Breakfit searches for two linear functions that are joined at the break point. To determine the break points, the model is fitted to the data applying an ordinary least-squares method with a brute-force search for the break points. A measure of the uncertainty of the break points is based on 2,000-block bootstrap simulations, applying a moving block bootstrap algorithm with a block length of 1. We were searching for two break points in the time intervals between 16 and 13 kyr BP. The two subintervals (one for each break point) were ranging from the outer boundary next to the break point of interest to the other break point. Subintervals were finally identified after at least two iterative applications to (in kyr BP): break point 1 [15.74, 14.45] and break point 2 [14.67, 13.16]. Breakfit identified the start in the $\Delta^{14}C$ drop at 14.66 ± 0.07 kyr BP followed by its decline by 54 ± 8‰ within 207 ± 95 years. Because of the very distinct dynamics of atmospheric $\Delta^{14}C$ including a rebound after its minimum (that is, after the carbon release to the atmosphere stopped), we also analysed the data more subjectively with a non-linear approach. Here we only calculated the mean time and mean $\Delta^{14}C$ right at the start of the carbon cycle changes around 14.6 kyr BP (two data points) and at its minimum (eight data points) assuming that $\Delta^{14}C$ followed a non-linear pathway between both and included a rebound thereafter. The $\Delta^{14}C$ data then starts to decline at 14.59 ± 0.04 kyr BP and stop after 258 ± 53 years with a maximum drop of 58 ± 14‰ followed by a rebound of atmospheric $\Delta^{14}C$. This non-linear dynamic is seen in the Tahiti data but also in our carbon cycle simulations (Figs 2 and 4a). Combining the linear and non-linear approach brings high confidence that the $\Delta^{14}C$ drop started at around 14.6 kyr BP. All uncertainties are given as 1σ.

Possible $\Delta^{14}C$ signature of permafrost carbon. The maximum possible $\Delta(\Delta^{14}C)$ of carbon released from permafrost thawing is a function of age and of atmospheric $\Delta^{14}C$ during time of production. From the $\Delta^{14}C$ signature (IntCal13) (ref. 9) of the precursor material (atmospheric CO_2), which varies before the B/A roughly between 250 and 550‰ (Fig. 6a), we first subtract the mean $\Delta^{14}C$ value of

terrestrial carbon at the LGM in the model (-50‰) before a further reduction in $\Delta^{14}C$ signature is realised by the radioactive decay of ^{14}C (half-life time of 5,730 years).

Carbon cycle model. We use the carbon cycle box model BICYCLE in transient mode to simulate changes in atmospheric CO_2 and $\Delta^{14}C$. The model setup is identical to an earlier study, which already proposed the magnitude of the CO_2 overshoot during the B/A[6].

We simulate the release of 125 Pg of carbon into the atmosphere with a constant rate that varies inversely with the time length of the event between 0.42 Pg C per year (300 years) and 2.5 Pg C per year (50 years) and configured the AMOC in either its strong or its weak mode. Both AMOC configurations differ in the strength of the overturning cell in the Atlantic with 16 Sv deep water production in the North Atlantic in the strong mode and 2 Sv in the weak mode. We repeated our previous comparison[6] of simulated atmospheric $\delta^{13}CO_2$ to ice core data from the EDC because new $\delta^{13}CO_2$ data were published in the mean time[1]. For this model-data comparison of $\delta^{13}CO_2$, we distinguished terrestrial and marine sources of the released carbon by assuming a $\delta^{13}C$ signature of -22.5 and -8.5‰, respectively (Fig. 3b). More details on these assumptions are found in our previous article[6]. $\Delta(\Delta^{14}C)$ of the simulated carbon release is depleted with respect to the atmosphere between -50 and $-1,250$‰. Initial conditions of ^{14}C production rates influence simulated $\Delta^{14}C$ over several ten thousand years[32]. All simulations therefore start at 60 kyr BP. In our standard case, ^{14}C production rates are assumed to be constant and 15% higher than present day, leading to atmospheric $\Delta^{14}C$ of $+250$‰ at 14.6 kyr BP in agreement with IntCal13 (ref. 9). Long-term trends in ^{14}C production rate as suggested by the geomagnetic field data[32] only slightly impact our simulations (Supplementary Fig. 4).

For model evaluation, BICYCLE is (a) compared in its oceanic carbon uptake dynamic resulting in a model-specific airborne fraction with other models, (b) used to simulate the Suess effect (years 1820–1950 AD), (c) the bomb ^{14}C peak (years 1950–2000 AD) and (d) applied on CO_2 release experiments for preindustrial background conditions. The model is compared with the results from another carbon cycle box model[66] (Suess effect and for preindustrial conditions) and with output from the GENIE model[67], an Earth system model of intermediate complexity (preindustrial conditions). All details on this model evaluation are found in the Supplementary Note 2 including Supplementary Figs 6–8.

Filtering true atmospheric CO_2 into signals recorded in EDC. The smoothing effect of the gas enclosure process in ice cores that transforms a potential true atmospheric CO_2 into a time series comparable to EDC ice core data is performed with a log-normal probability density function with an assumed mean value or width E of 400 ± 80 years (mean $\pm 1\sigma$)[6] (Supplementary Fig. 2c):

$$f(x) = \frac{1}{x \cdot \sigma \cdot \sqrt{2\pi}} \cdot e^{-0.5\left(\frac{\ln(x)-\mu}{\sigma}\right)^2} \tag{1}$$

with x (in years) as the time elapsed since the last exchange with the atmosphere. From the two free parameters, μ and σ of the equation, we chose for simplicity $\sigma = 1$, which leads to $E = e^{\mu - 0.5}$. The application of such a filter function for the transformation of true atmospheric signals into those that might be recorded in ice cores during rapid climate change was compared with results from firn densification models and extensively validated with CH_4 data from both hemispheres[6].

References

1. Schmitt, J. *et al.* Carbon isotope constraints on the deglacial CO_2 rise from ice cores. *Science* **336**, 711–714 (2012).
2. Skinner, L. C., Fallon, S., Waelbroeck, C., Michel, E. & Barker, S. Ventilation of the deep Southern Ocean and deglacial CO_2 Rise. *Science* **328**, 1147–1151 (2010).
3. Parrenin, F. *et al.* Synchronous change in atmospheric CO_2 and Antarctic temperature during the last deglacial warming. *Science* **339**, 1060–1063 (2013).
4. Veres, D. *et al.* The Antarctic ice core chronology (AICC2012): an optimized multi-parameter and multi-site dating approach for the last 120 thousand years. *Clim. Past* **9**, 1733–1748 (2013).
5. Baumgartner, M. *et al.* High-resolution interpolar difference of atmospheric methane around the Last Glacial Maximum. *Biogeosciences* **9**, 3961–3977 (2012).
6. Köhler, P., Knorr, G., Buiron, D., Lourantou, A. & Chappellaz, J. Abrupt rise in atmospheric CO_2 at the onset of the Bølling/Allerød: in-situ ice core data versus true atmospheric signals. *Clim. Past* **7**, 473–486 (2011).
7. Durand, N. *et al.* Comparison of ^{14}C and U-Th ages in corals from IODP #310 cores offshore Tahiti. *Radiocarbon* **55**, 1947–1974 (2013).
8. Barker, S. *et al.* 800,000 Years of abrupt climate variability. *Science* **334**, 347–351 (2011).
9. Reimer, P. J. *et al.* IntCal13 and Marine13 radiocarbon age calibration curves 0-50,000 years cal BP. *Radiocarbon* **55**, 1869–1887 (2013).
10. Hoffmann, D. L. *et al.* Towards radiocarbon calibration beyond 28 ka using speleothems from the Bahamas. *Earth Planet. Sci. Lett.* **289**, 1–10 (2010).
11. Southon, J., Noronha, A. L., Cheng, H., Edwards, R. L. & Wang, Y. A high-resolution record of atmospheric ^{14}C based on Hulu Cave speleothem H82. *Quaternary Sci. Rev.* **33**, 32–41 (2012).
12. Hughen, K., Southon, J., Lehman, S., Bertrand, C. & Turnbull, J. Marine-derived ^{14}C calibration and activity record for the past 50,000 years updated from the Cariaco Basin. *Quaternary Sci. Rev.* **25**, 3216–3227 (2006).
13. Noronha, A. L. *et al.* Assessing influences on speleothem dead carbon variability over the Holocene: implications for speleothem-based radiocarbon calibration. *Earth Planet. Sci. Lett.* **394**, 20–29 (2014).
14. Bronk Ramsey, C. *et al.* A complete terrestrial radiocarbon record for 11.2 to 52.8 kyr B.P. *Science* **338**, 370–374 (2012).
15. Bard, E. Correction of accelerator mass spectrometry ^{14}C ages measured in planktonic foraminifera: paleoceanographic implications. *Paleoceanography* **3**, 635–645 (1988).
16. Gong, X., Knorr, G., Lohmann, G. & Zhang, X. Dependence of abrupt Atlantic meridional ocean circulation changes on climate background states. *Geophys. Res. Lett.* **40**, 3698–3704 (2013).
17. Butzin, M., Prange, M. & Lohmann, G. Readjustment of glacial radiocarbon chronologies by self-consistent three-dimensional ocean circulation modeling. *Earth Planet. Sci. Lett.* **317-318**, 177–184 (2012).
18. Singarayer, J. S. *et al.* An oceanic origin for the increase of atmospheric radiocarbon during the Younger Dryas. *Geophys. Res. Lett.* **35**, L14707 (2008).
19. Capron, E. *et al.* Glacial-interglacial dynamics of Antarctic firn columns: comparison between simulations and ice core air $\delta^{15}N$ measurements. *Clim. Past* **9**, 983–999 (2013).
20. Freitag, J., Kipfstuhl, J., Laepple, T. & Wilhelms, F. Impurity-controlled densification: a new model for stratified polar firn. *J. Glaciol.* **59**, 1163–1169 (2013).
21. Rosen, J. L. *et al.* An ice core record of near-synchronous global climate changes at the Bølling transition. *Nat. Geosci.* **7**, 459–463 (2014).
22. Monnin, E. *et al.* Atmospheric CO_2 concentrations over the last glacial termination. *Science* **291**, 112–114 (2001).
23. Rasmussen, S. O. *et al.* A new Greenland ice core chronology for the last glacial termination. *J. Geophys. Res.* **111**, D06102 (2006).
24. Steffensen, J. P. *et al.* High-resolution Greenland ice core data show abrupt climate change happens in few years. *Science* **321**, 680–684 (2008).
25. Neftel, A., Oeschger, H., Staffelbach, T. & Stauffer, B. CO_2 record in the Byrd ice core 50,000-5,000 years BP. *Nature* **331**, 609–611 (1988).
26. Smith, H. J., Fischer, H., Wahlen, M., Mastroianni, D. & Deck, B. Dual modes of the carbon cycle since the Last Glacial Maximum. *Nature* **400**, 248–250 (1999).
27. Ahn, J. *et al.* A record of atmospheric CO_2 during the last 40,000 years from the Siple Dome, Antarctica ice core. *J. Geophys. Res.* **109**, D13305 (2004).
28. Pedro, J. B., Rasmussen, S. O. & van Ommen, T. D. Tightened constraints on the time-lag between Antarctic temperature and CO_2 during the last deglaciation. *Clim. Past* **8**, 1213–1221 (2012).
29. Marchitto, T. M., Lehman, S. J., Oritz, J. D., Flückiger, J. & van Geen, A. Marine radiocarbon evidence for the mechanism of deglacial atmospheric CO_2 rise. *Science* **316**, 1456–1459 (2007).
30. Stott, L., Southon, J., Timmermann, A. & Koutavas, A. Radiocarbon age anomaly at intermediate water depth in the Pacific Ocean during the last deglaciation. *Paleoceanography* **24**, PA2223 (2009).
31. Deschamps, P. *et al.* Ice-sheet collapse and sea-level rise at the Bolling warming 14,600 years ago. *Nature* **483**, 559–564 (2012).
32. Köhler, P., Muscheler, R. & Fischer, H. A model-based interpretation of low frequency changes in the carbon cycle during the last 120 000 years and its implications for the reconstruction of atmospheric $\Delta^{14}C$. *Geochem. Geophys. Geosyst.* **7**, Q11N06 (2006).
33. Kindler, P. *et al.* Temperature reconstruction from 10 to 120 kyr b2k from the NGRIP ice core. *Clim. Past* **10**, 887–902 (2014).
34. Gorham, E., Lehman, C., Dyke, A., Clymo, D. & Janssens, J. Long-term carbon sequestration in North American peatlands. *Quaternary Sci. Rev.* **58**, 77–82 (2012).
35. Sowers, T. Late Quaternary atmospheric CH_4 isotope record suggests marine clathrates are stable. *Science* **311**, 838–840 (2006).
36. Fischer, H. *et al.* Changing boreal methane sources and constant biomass burning during the last termination. *Nature* **452**, 864–867 (2008).
37. Möller, L. *et al.* Independent variations of CH_4 emissions and isotopic composition over the past 160,000 years. *Nat. Geosci.* **6**, 885–890 (2013).
38. Schaphoff, S. *et al.* Contribution of permafrost soils to the global carbon budget. *Environ. Res. Lett.* **8**, 014026 (2013).
39. Liu, Z. *et al.* Transient simulation of last deglaciation with a new mechanism for Bølling-Allerød warming. *Science* **325**, 310–314 (2009).
40. Ciais, P. *et al.* Large inert carbon pool in the terrestrial biosphere during the Last Glacial Maximum. *Nat. Geosci.* **5**, 74–79 (2012).
41. Saito, K. *et al.* LGM permafrost distribution: how well can the latest PMIP multi-model ensembles reconstruct? *Clim. Past* **9**, 1697–1714 (2013).

42. Vandenberghe, J. *et al.* The Last Permafrost Maximum (LPM) map of the Northern Hemisphere: permafrost extent and mean annual air temperatures, 25–17 ka BP. *Boreas* **43,** 652–666 (2014).

43. Koven, C. D. *et al.* Permafrost carbon-climate feedbacks accelerate global warming. *Proc. Natl Acad. Sci. USA* **108,** 14769–14774 (2011).

44. Schuur, E. *et al.* Expert assessment of vulnerability of permafrost carbon to climate change. *Clim. Change* **119,** 359–374 (2013).

45. Petrenko, V. V. *et al.* $^{14}CH_4$ measurements in Greenland ice: investigating last glacial termination CH_4 sources. *Science* **324,** 506–508 (2009).

46. Rostek, F. & Bard, E. Hydrological changes in eastern Europe during the last 40,000 years inferred from biomarkers in Black Sea sediments. *Quaternary Res.* **80,** 502–509 (2013).

47. Ridgwell, A., Maslin, M. & Kaplan, J. O. Flooding of the continental shelves as a contributor to deglacial CH_4 rise. *J. Quaternary Sci.* **27,** 800–806 (2012).

48. Weber, M. E. *et al.* Millennial-scale variability in Antarctic ice-sheet discharge during the last deglaciation. *Nature* **510,** 134–138 (2014).

49. Clark, P. U., Mitrovica, J. X., Milne, G. A. & Tamisiea, M. E. Sea-level fingerprinting as a direct test for the source of global meltwater pulse IA. *Science* **295,** 2438–2441 (2002).

50. Smith, W. H. & Sandwell, D. T. Global sea floor topography from satellite altimetry and ship depth soundings. *Science* **277,** 1956–1962 (1997).

51. Strauss, J. *et al.* The deep permafrost carbon pool of the Yedoma region in Siberia and Alaska. *Geophys. Res. Lett.* **40,** 6165–6170 (2013).

52. Vonk, J. E. *et al.* Activation of old carbon by erosion of coastal and subsea permafrost in Arctic Siberia. *Nature* **489,** 137–140 (2012).

53. Feng, X. *et al.* Differential mobilization of terrestrial carbon pools in Eurasian Arctic river basins. *Proc. Natl Acad. Sci. USA* **110,** 14168–14173 (2013).

54. WAIS Divide Project Members. Onset of deglacial warming in West Antarctica driven by local orbital forcing. *Nature* **500,** 440–444 (2013).

55. Ahn, J. & Brook, E. J. Atmospheric CO_2 and climate on millennial time scales during the last glacial period. *Science* **322,** 83–85 (2008).

56. Zhang, X., Lohmann, G., Knorr, G. & Xu, X. Different ocean states and transient characteristic in Last Glacial Maximum simulations and implications for deglaciation. *Clim. Past* **9,** 2319–2333 (2013).

57. Barker, S. & Knorr, G. Antarctic climate signature in the Greenland ice core record. *Proc. Natl Acad. Sci. USA* **104,** 17278–17282 (2007).

58. Lourantou, A., Chappellaz, J., Barnola, J.-M., Masson-Delmotte, V. & Raynaud, D. Changes in atmospheric CO_2 and its carbon isotopic ratio during the penultimate deglaciation. *Quaternary Sci. Rev.* **29,** 1983–1992 (2010).

59. Schneider, R., Schmitt, J., Köhler, P., Joos, F. & Fischer, H. A reconstruction of atmospheric carbon dioxide and its stable carbon isotopic composition from the penultimate glacial maximum to the last glacial inception. *Clim. Past* **9,** 2507–2523 (2013).

60. Masson-Delmotte, V. *et al.* Abrupt change of Antarctic moisture origin at the end of Termination II. *Proc. Natl Acad. Sci.* **107,** 12091–12094 (2010).

61. Landais, A. *et al.* Two-phase change in CO_2, Antarctic temperature and global climate during Termination II. *Nat. Geosci.* **6,** 1062–1065 (2013).

62. Stenni, B. *et al.* Expression of the bipolar see-saw in Antarctic climate records during the last deglaciation. *Nat. Geosci.* **4,** 46–49 (2011).

63. Buiron, D. *et al.* Regional imprints of millennial variability during the MIS 3 period around Antarctica. *Quaternary Sci. Rev.* **48,** 99–112 (2012).

64. Khvorostovsky, D. V. *et al.* Vulnerability of permafrost carbon to global warming. Part II: sensitivity of permafrost carbon stock to global warming. *Tellus B* **60,** 265–275 (2008).

65. Mudelsee, M. Break function regression. *Eur. Phys. J. Spec. Top.* **174,** 49–63 (2009).

66. Bard, E., Raisbeck, G. M., Yiou, F. & Jouzel, J. Solar modulation of cosmogenic nuclide production over the last millennium: comparison between ^{14}C and ^{10}Be records. *Earth Planet. Sci. Lett.* **150,** 453–462 (1997).

67. Cao, L. *et al.* The role of ocean transport in the uptake of anthropogenic CO_2. *Biogeosciences* **6,** 375–390 (2009).

68. Lourantou, A. *et al.* Constraint of the CO_2 rise by new atmospheric carbon isotopic measurements during the last deglaciation. *Global Biogeochem. Cycles* **24,** GB2015 (2010).

69. EPICA-community-members. One-to-one coupling of glacial climate variability in Greenland and Antarctica. *Nature* **444,** 195–198 (2006).

70. NGRIP Members. High-resolution record of Northern Hemisphere climate extending into the last interglacial period. *Nature* **431,** 147–151 (2004).

Acknowledgements

Author contributions

All authors designed research; P.K. performed carbon cycle simulations with BICYCLE; E.B. performed carbon cycle simulations with other box models; G.K. performed climate simulations; P.K. drafted the manuscript with contributions from all co-authors.

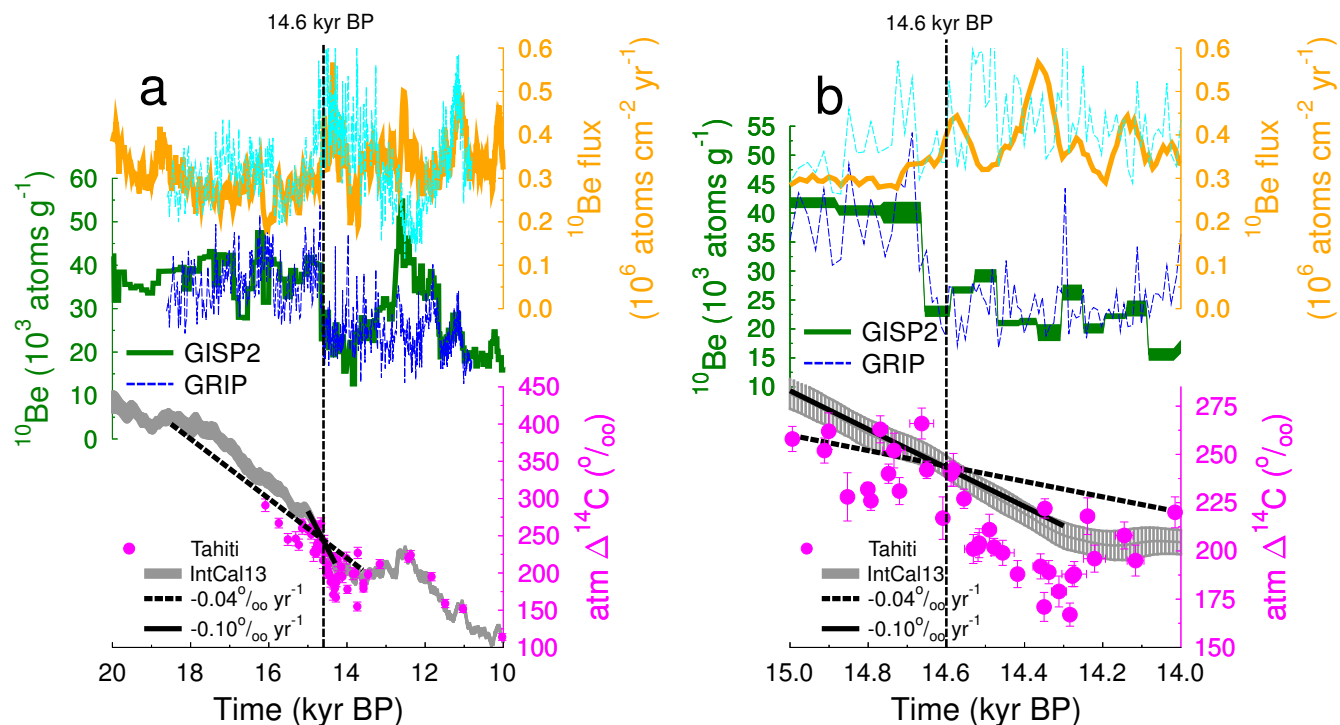## Additional information

Supplementary Figure 1: Comparing atmospheric [10]Be and Δ^{14}C data to evaluate the potential impact of variable ^{14}C production rates on Δ^{14}C. (a) Termination I. (b) Focus on 15 to 14 kyr BP. [10]Be fluxes and concentration of Greenland ice cores GISP2[1] (bold closed lines, green and orange) and GRIP[2] (dashed lines, blue and cyan) on GICC05[3] age model. Atmospheric Δ^{14}C from IntCal13[4] (grey band of $\pm 1\sigma$ around the mean) and Tahiti corals[5] (magenta, $\pm 1\sigma$ in both age and Δ^{14}C) including a linear trend with $-0.04‰$ yr^{-1} or $-0.10‰$ yr^{-1}.
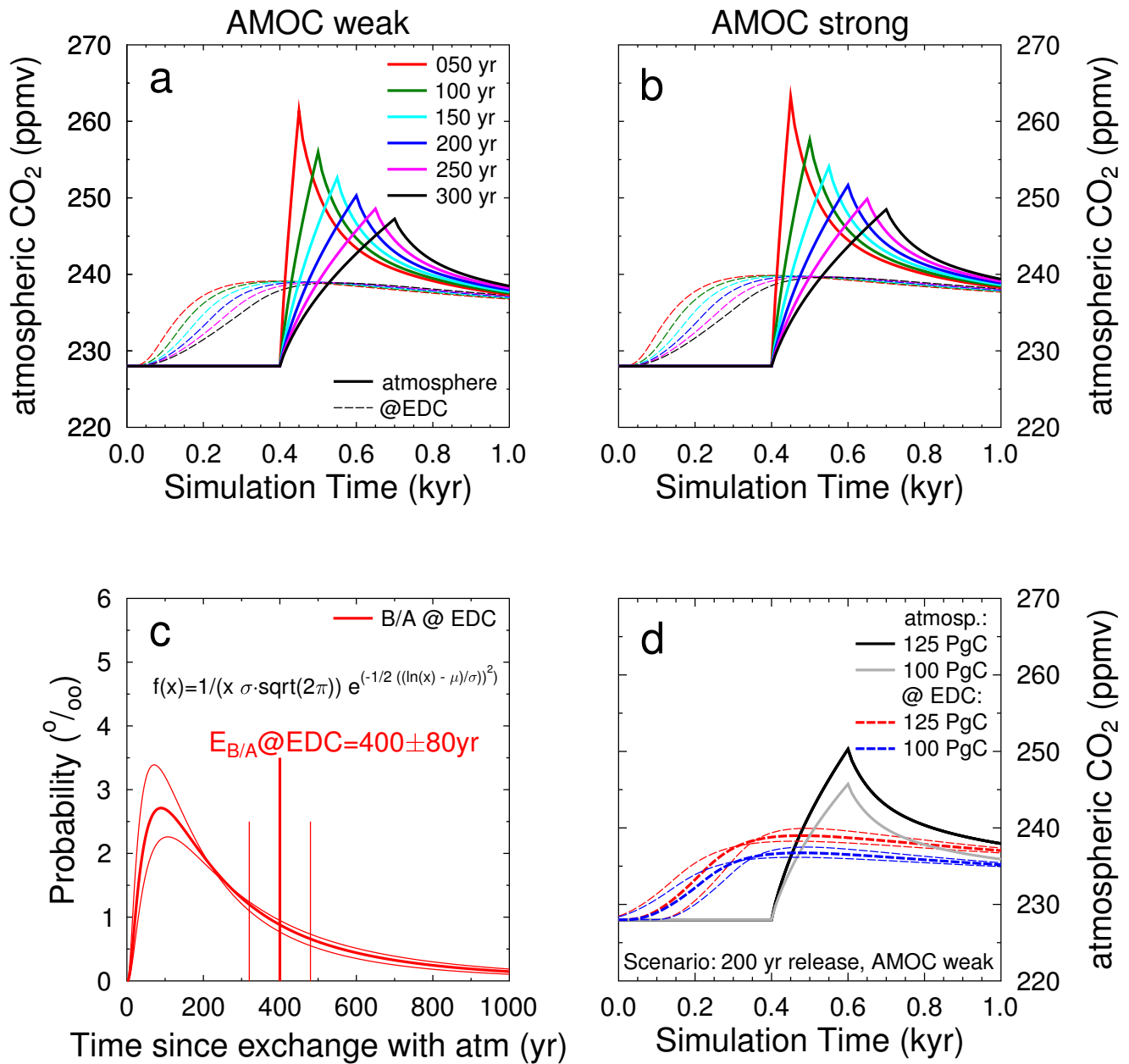
Supplementary Figure 2: Simulated changes in atmospheric CO_2 using the BICYCLE carbon cycle model. The model is set-up for around 14.6 kyr BP. Simulations vary in the length of the carbon release between 50 yr and 300 yr, AMOC is (a) weak or (b) strong. Both the atmospheric signal (bold) and the smoothed signal (dashed) that would be recorded in EDC are plotted. No age correction during smoothing is applied. (c) The atmospheric time series are filtered (smoothed) to address the firn air mixing before gas enclosure in ice cores with a log-normal probability density (PDF) function, that was tested with output of firn densification models[6]. The mean width E of PDF corresponds to the climatic conditions around 14.6 kyr BP at EDC ($E = 400 \pm 80$ years (1σ)). The PDF follows Equation 1 shown in the methods (main text), in which μ was chosen in order to follow $E = e^{\mu - 0.5}$ for the given mean width $E = 400$ years (bold lines) or 320 and 480 year, respectively (thin lines). (d) Comparing how the true atmospheric CO_2 signal in two scenarios (125 or 100 PgC released in 200 years, AMOC off) might be recorded in EDC including the 1σ uncertainty in the log-normal PDF (subfigure c) used for smoothing during gas enclosure.

2
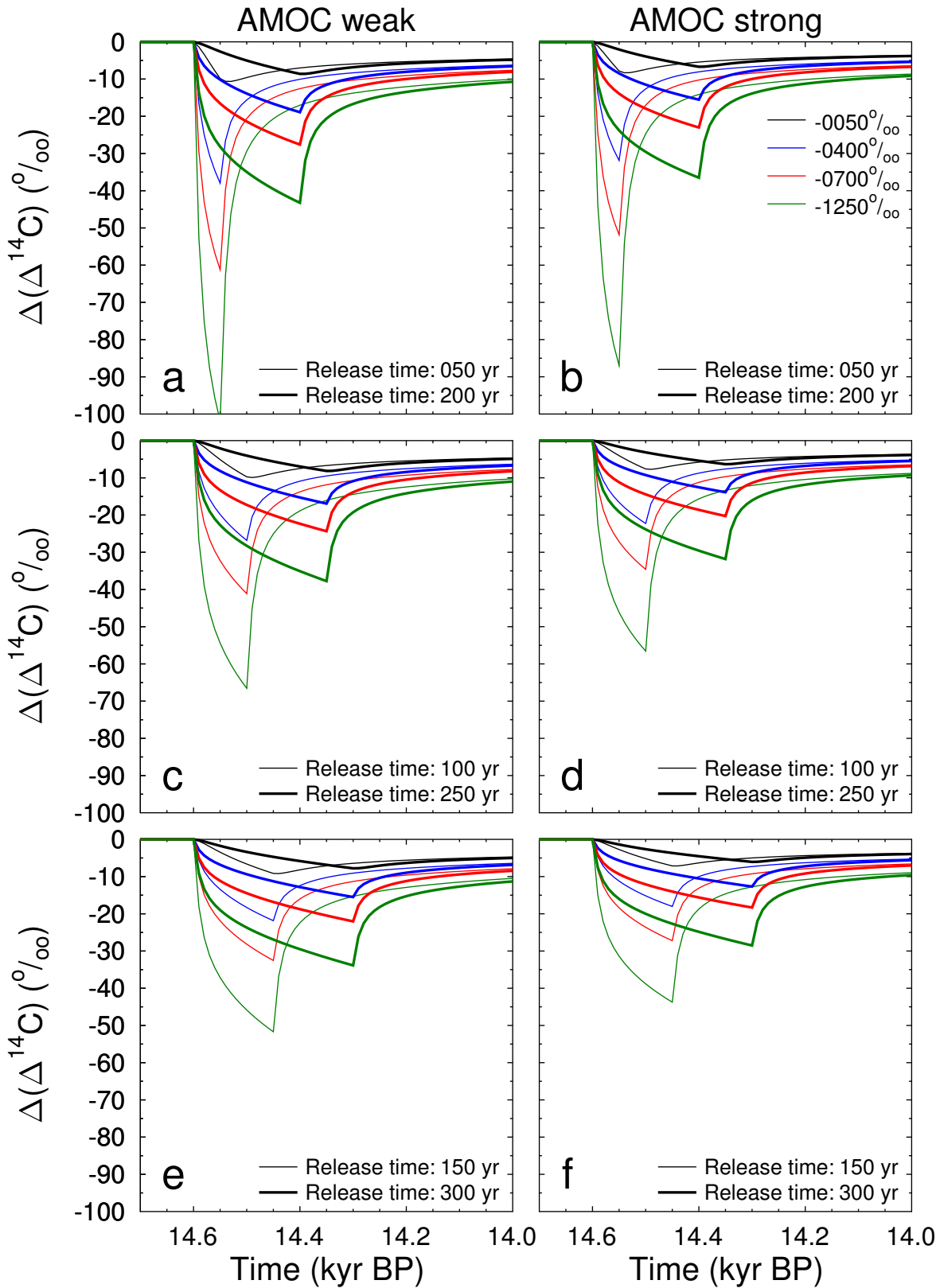
Supplementary Figure 3: Simulated changes in atmospheric Δ^{14}C using the BICYCLE carbon cycle model. The model is set-up for around 14.6 kyr BP. Simulations vary in the length of the carbon release: a,b) 50 and 200 years; c,d) 100 and 250 years; e,f) 150 and and 300 years. AMOC is weak (left) or strong (right), and ^{14}C depletion of released carbon with respect to atmosphere varying between –50‰ and –1250‰. ^{14}C production rate was constant at $1.15\times$ pre-industrial level, which gives after 45 kyr of spin-up time an atmospheric Δ^{14}C of about 250‰, comparable with the observations.
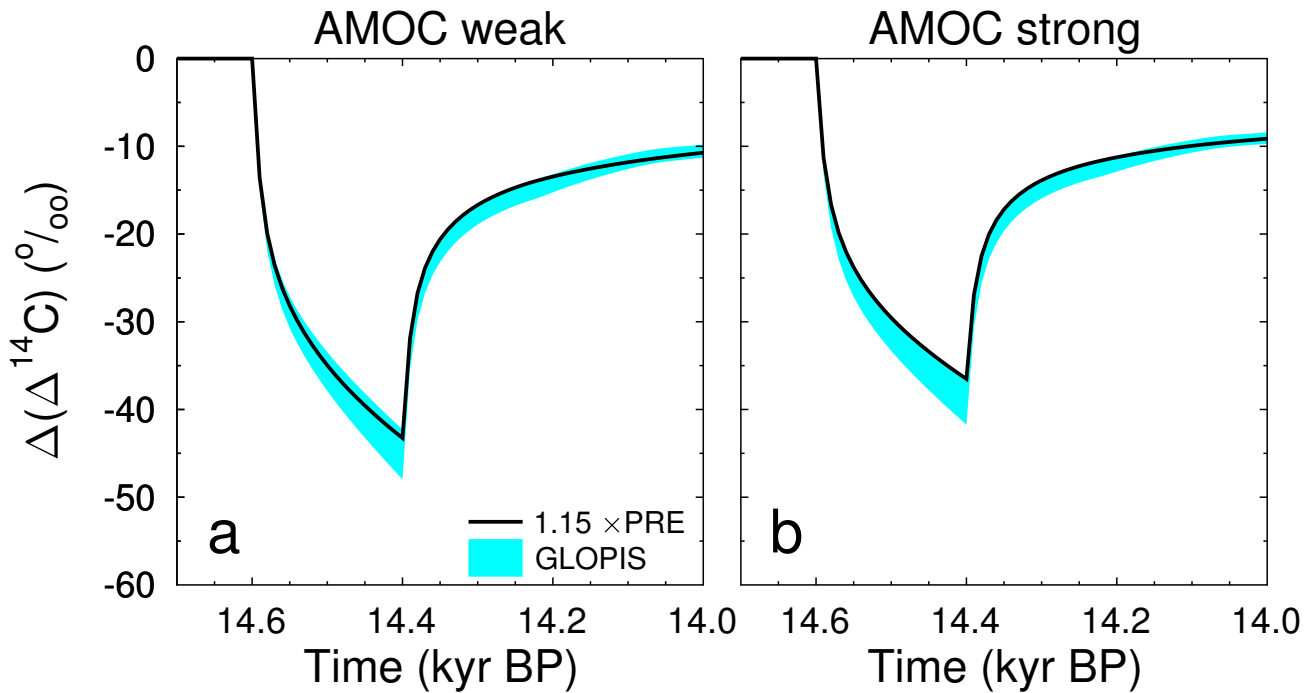
Supplementary Figure 4: Impact of long-term change in ^{14}C production rate on simulated atmospheric Δ^{14}C. The ^{14}C production rate were derived from the geomagnetic field (GLOPIS) and applied in the BICYCLE model as in a previous application[7]. Results for our best guess scenario (-1250‰, 125 Pg carbon released in 200 years) with 45 kyr of spin-up time are shown. AMOC is in (a) weak or (b) strong mode. Cyan band spans results based on either a minimum or a maximum change in ^{14}C production rate as deduced from GLOPIS[7].
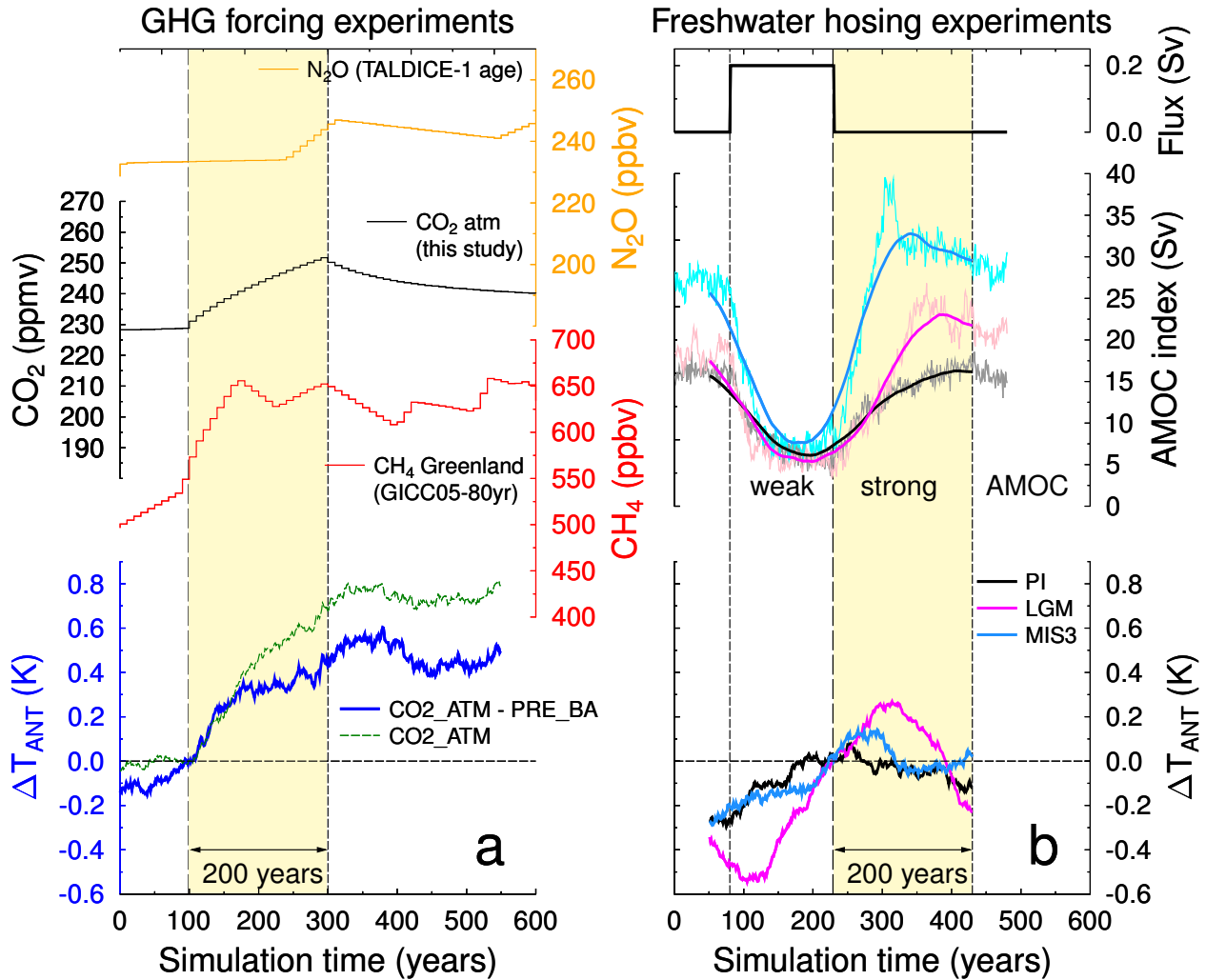
Supplementary Figure 5: Results of transient climate model simulations using COSMOS. Shown are the simulated annual mean Antarctic surface temperature change ΔT_{ANT} in (a) our GHG forcing experiments and (b) a reanalysis of North Atlantic freshwater hosing experiments[8,9], which serve as a surrogate for the simulation of abrupt climate changes. Recently it has been shown that the recovery and amplification of the AMOC at the end of freshwater perturbations is strongly dependent on the climate background state[8]. Therefore we analysed the Antarctic temperature response for three different climate states (PI: pre-industrial; LGM: Last Glacial Maximum at 21 kyr BP; MIS3: 32 kyr BP) that cover a wide spectrum of glacial-interglacial conditions to evaluate the robustness of the Antarctic temperature response. In Panel (a) we show the GHG N_2O, CO_2 and CH_4 as used for forcing the model in simulation CO2_ATM and the simulated anomaly in ΔT_{ANT} in scenario CO2_ATM (green dashed) and of CO2_ATM–PRE_BA (blue), both as 100 years running averages with respect to year 100. Vertical lines bracket the rise in atmospheric CO_2, representing 14.6 and 14.4 kyr BP, respectively. In panel (b) the North Atlantic freshwater hosing is shown in Sv (1 Sv = 10^6 m^3 s^{-1}). The freshwater perturbation with a freshwater flux of 0.2 Sv is added to the ice-rafted debris belt in the North Atlantic Ocean, around 40°N – 55°N, 45°W – 20°W of the central Atlantic Ocean. The intensity of the AMOC is presented by the maximum value of the meridional overturning stream function of the upper 200–3000 m and 30°N northward[8]. The simulated anomaly in ΔT_{ANT} for the different background climate states are shown as 100 years running averages with respect to year 230 (i.e. the end of the freshwater perturbation). Hence the corresponding key intervals marked in apricot background colour in panel a) and b) are between 100-300 years and 230-430, respectively.
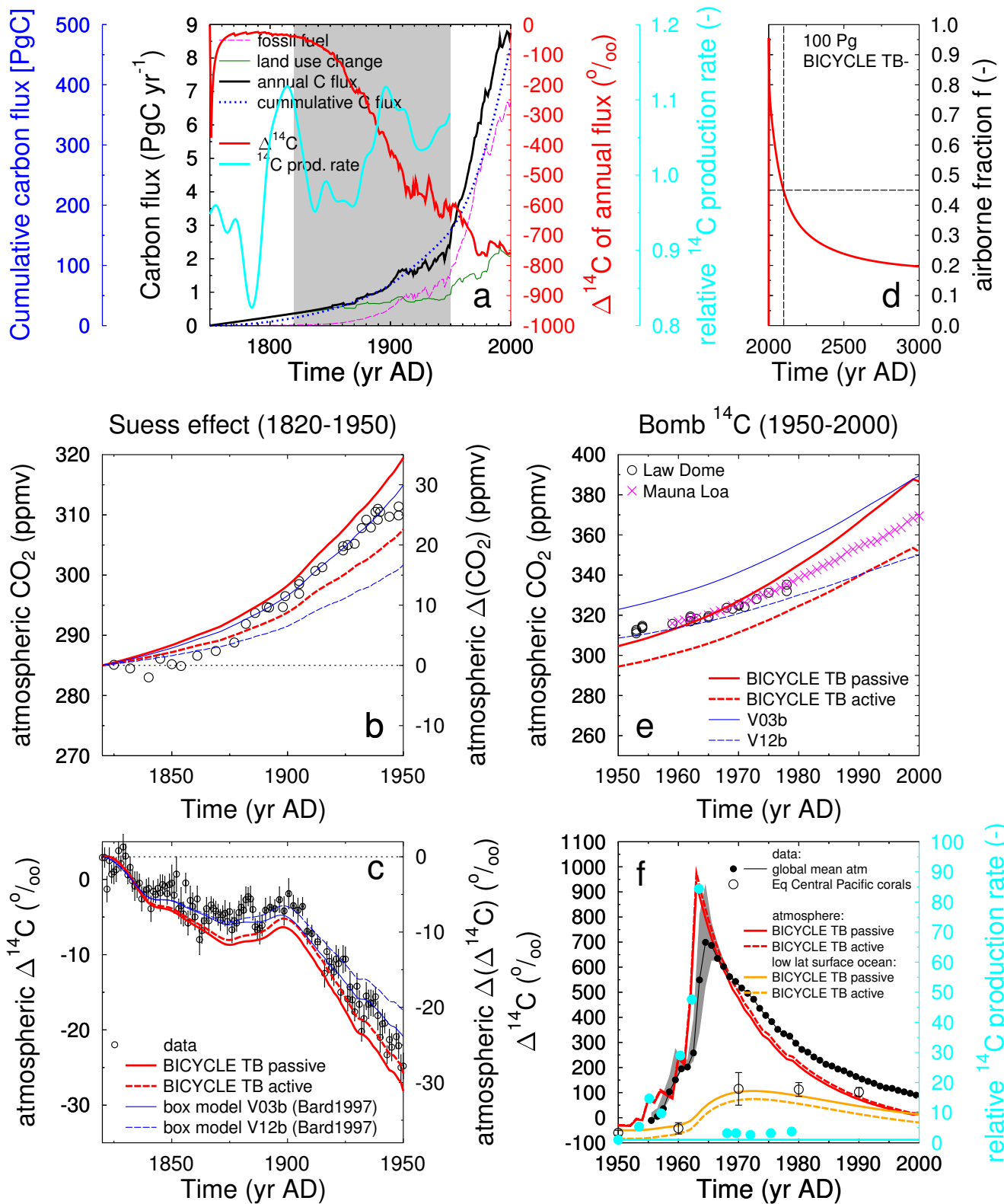
5

Supplementary Figure 6: Evaluation of ^{14}C model performance for Suess effect and bomb ^{14}C peak. See caption on the following page.

Supplementary Figure 6: Evaluation of ^{14}C model performance for Suess effect and bomb ^{14}C peak.
(a) Fluxes of fossil fuel emissions[10] (magenta), and land use change[11] (green, between 1850 AD and 1750 AD linearly extrapolated to zero). Assumption for Δ^{14}C signature of total anthropogenic C flux to the atmosphere (red): Land use change extracts woody parts of trees (fractionated by $-40‰$ during photosynthesis from atmosphere, no further ageing), fossil fuels are ^{14}C-free (Δ^{14}C$= -1000‰$). Relative changes in ^{14}C production rate (cyan) with respect to the long-term Holocene[12]. Gray box (1820–1950 AD) covers bomb-free Suess effect data[13]. (b) Simulated changes in atmospheric CO_2 against CO_2 data from the Law Dome ice core[14] (circles). BICYCLE model (red) with terrestrial biosphere (TB) either passive (constant, solid lines) or active (changes as function of CO_2, dashed lines). A second box model in two different versions (blue) for comparison[15]. (c) Simulated changes in atmospheric Δ^{14}C against reconstructions (circles with error bars (1σ)[13]). BICYCLE started from 10 kyr BP, the 12-box model started at 0 AD, both used the same relative ^{14}C production rate changes[12]. (d) Airborne fraction f over time for the injection of 100 PgC in year 2001 (background CO_2 of 389 ppmv) in BICYCLE with terrestrial biosphere passive (TB-). No fossils fuel emission after year 2000. f is calculated from the difference to simulation without 100 PgC injection for the next 1000 years. Dotted lines mark f after 100 years. (e) Simulated atmospheric CO_2 in the bomb ^{14}C-peak time window (1950–2000 AD) against CO_2 data (Law Dome[14], Mauno Loa CO_2 annual mean[16]). (f) Simulated bomb ^{14}C-peak against reconstructions. Assumed additional bomb-related ^{14}C production rate calculated after Naegler[17], but normalised to the mean natural ^{14}C production rate used here (85% of Naegler[17]) leading to the input of $1.2 \cdot 10^6$g ^{14}C into the atmosphere. Atmospheric ^{14}C data[18] (global mean (black filled circles) with range measured in high latitude northern hemisphere and southern hemisphere (grey area) and coral-based reconstructions of central equatorial Pacific surface waters[19] (open circles with error bars denoting the observed range) against simulations with BICYCLE.
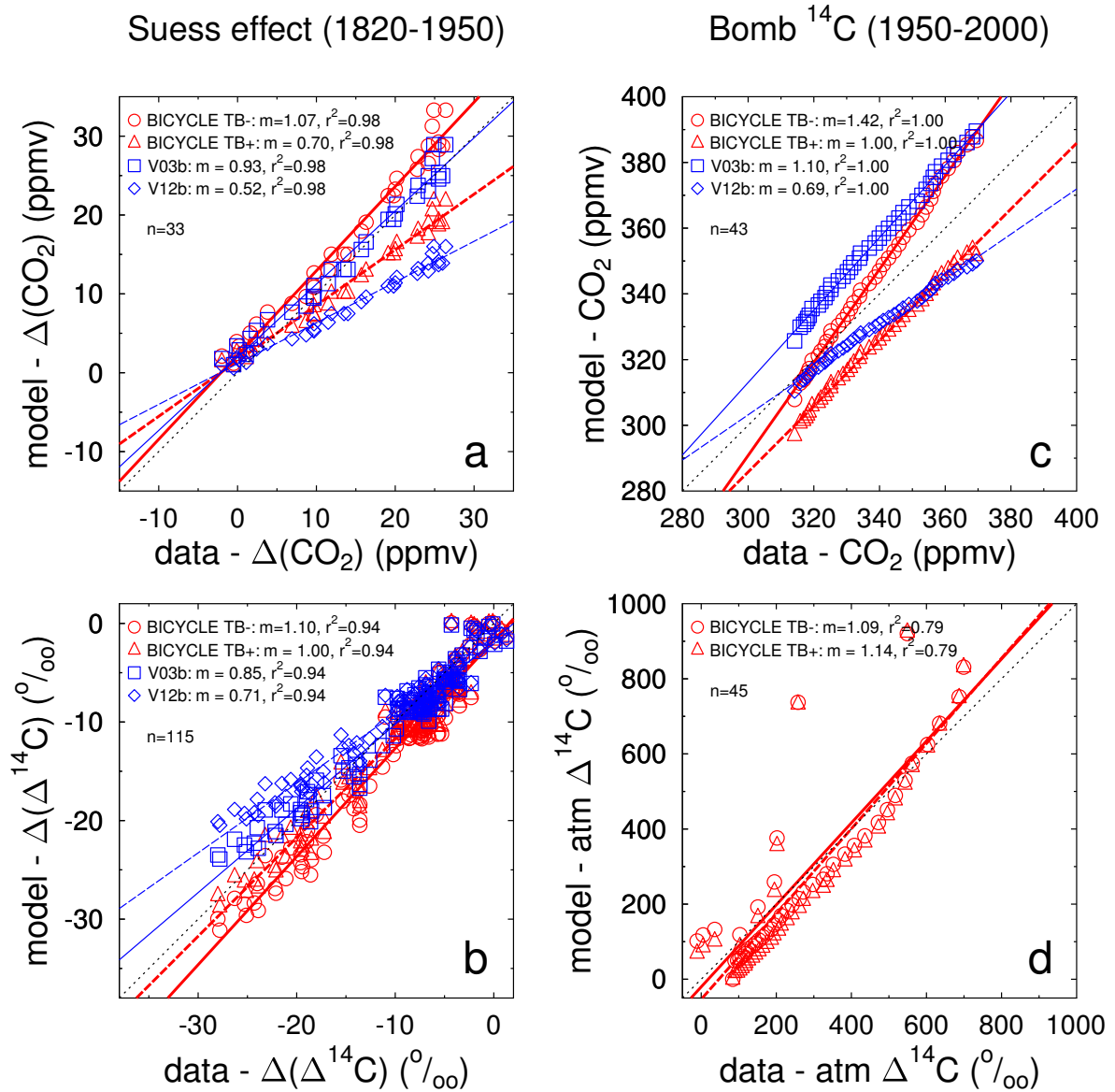
Supplementary Figure 7: Suess effect and bomb ^{14}**C peak.** Scatter plots of model-data comparison for changes in atmospheric CO_2 and $\Delta^{14}C$ for the Suess effect and the bomb ^{14}C peak. (a) Atmospheric CO_2 for the Suess effect. (b) Atmospheric $\Delta^{14}C$ for the Suess effect. (c) Atmospheric CO_2 for the bomb ^{14}C peak. (d) Atmospheric $\Delta^{14}C$ for the bomb ^{14}C peak. Model results are resampled only for the n years in which data points are available. The dotted black lines denotes the perfect model-data agreement (slope $m = 1.0$). The calculated slopes m and the correlation coefficients r^2 of the linear regressions are contained in the legends.
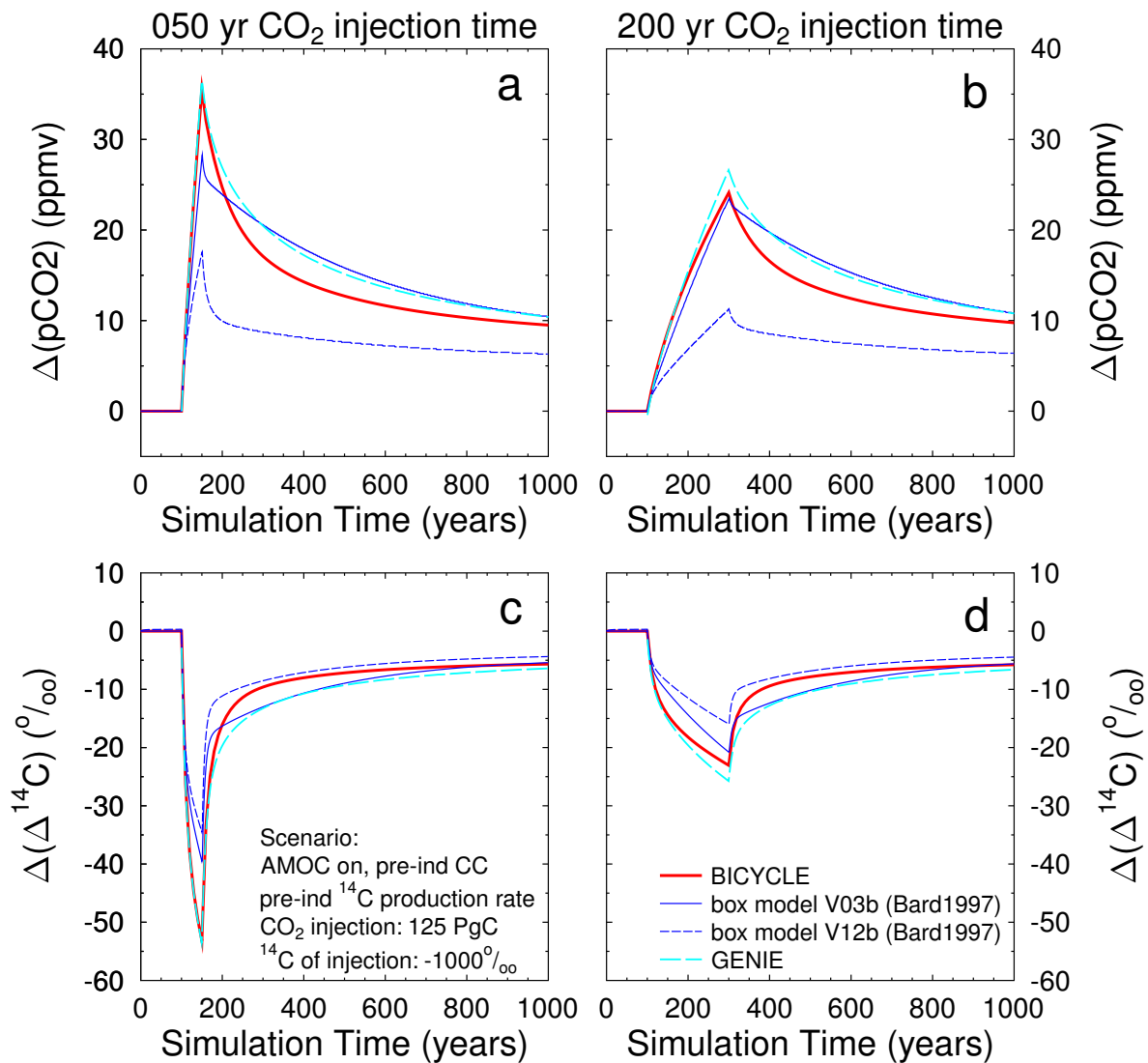
Supplementary Figure 8: Comparing different carbon cycle models. BICYCLE (red), the other box model[15] (blue, two versions), and the Earth System model of intermediate complexity GENIE[20] (cyan) are compared for a pre-industrial CO_2 injection scenario (AMOC strong, pre-industrial carbon cycle, pre-industrial ^{14}C production rate) for 125 PgC injection with ^{14}C signature of $-1000‰$. Injection started in simulation year 100 for a length of 50 (left) or 200 (right) years. Top: Changes in atmospheric CO_2, bottom: changes in atmospheric $\Delta^{14}C$.

9

Supplementary Note 1

Atmospheric Δ^{14}C Data. Atmospheric Δ^{14}C deduced from corals might be influenced by temporal changes in the reservoir ages, or by variable ^{14}C production rates. Both potential sources of uncertainty are briefly discussed below:

(a) Reservoir ages

Reservoir ages might vary with time due to changes in (i) ocean circulation or (ii) gas exchange rates[21]:

(i) Especially around the end of Heinrich Stadial 1 the resumption of the Atlantic meridional over-turning circulation (AMOC) might lead to variable reservoir ages. This leads, for example, for Atlantic sites in the Cariaco Basin in an ocean carbon cycle model to uncertainties and changes in the reservoir age of the order of 100 years within a few centuries[22]. This time-dependent change in reservoir age leads to a difference in atmospheric Δ^{14}C of less than 5‰ if compared to results based on a constant reservoir age. The influence of the AMOC resumption around 14.6 kyr BP on reservoir ages should be smaller in the central Pacific around Tahiti than in the Caribbean around Cariaco. Another simulation study[23] focusing on the impact of AMOC changes during the Younger Dryas also found rather constant reservoir ages throughout most of the Pacific. Furthermore, wind-driven circulation or ventilation might also impact on the reservoir age. However, as discussed in the next paragraph in detail we do not find any indication that surface wind speed around Tahiti was changing, it stayed remarkable stable in all simulation results which were available to us covering stable climates for modern times and LGM, and abrupt climate changes during MIS 3 and the last deglaciation (this study and [8,9]). Reservoir age changes based on ocean circulation change is therefore very small and thus negligible.

(ii) Gas exchange rates of CO_2 between atmosphere and surface ocean depend mainly on local wind speed. In existing simulations local surface wind speed around Tahiti (about $150°$W, $18°$S) are remarkable stable. In simulations with the COSMOS coupled Earth system model (see further below) surface wind speed around Tahiti never changes by more than 10% from its pre-industrial values. This is the case in simulation results for LGM climate[9], for our simulation scenarios PRE_BA and CO2_ATM (this study), or across an AMOC shutdown and resumption[8]. We therefore found no supporting evidence for a wind speed change in Tahiti across an abrupt stadial/interstadial transition comparable to the B/A around 14.6 kyr BP and therefore assume that the impact of reservoir age change on the interpretation of the coral-based Δ^{14}C data from Tahiti was small and negligible.

A recent study[24] used the same Δ^{14}C data from Tahiti corals to come to a different interpretation of the reservoir age. They assumed that the IntCal09 stack provides the true atmospheric Δ^{14}C signal, which implied that all differences in Tahiti Δ^{14}C to IntCal09 has to be explained by a variable reservoir age R. Consequently, they found R to vary up to 400 years at the onset of the B/A. This is the opposite to our interpretation. Here, we rely on the Tahiti corals to be the most reliable recorder of Δ^{14}C — because of its small measurement uncertainty and precise U/Th dating. One main concern about the work by Kubota et al.[24] is the usage of the old IntCal09 curve rather than the new updated version[4] IntCal13. Indeed, the main difference between the two IntCal curves occurs around the Heinrich 1 event with significant improvements included in the IntCal13 curve. This can be briefly illustrated with a simple example of an age within the Heinrich 1 event: 16,500 calendar years BP corresponds to 13,310 ^{14}C years BP in the IntCal09 curve, but

13,682 ^{14}C years BP in the new IntCal13 curve. Consequently, the use of IntCal13 instead of IntCal09 reduces automatically by 372 years the apparent ^{14}C reservoir age for a coral sample of that calendar age. This is the magnitude of the change in ΔR that is interpreted erroneously by Kubota et al.[24] (cf. their Fig. 4 and related text) as due to CO_2 release by the ocean.

(b) Changes in ^{14}C production rate

Atmospheric Δ^{14}C might also vary because of a change in ^{14}C production rate, which would also be visible in other cosmogenic isotopes, e.g. in the atmospheric concentration of ^{10}Be which is available from the GISP2 ice core[1] and in high resolution from the GRIP ice core[2]. GISP2 ^{10}Be data on the GICC05 chronology[3] show a decrease in ^{10}Be concentration by 50% around 14.65 kyr BP, but a gradual rise in the ^{10}Be flux (Supplementary Fig. 1). Depending on the kind of deposition (wet, dry) atmospheric ^{10}Be concentration is more related to either ^{10}Be concentration or ^{10}Be flux in ice cores. The patterns found in ^{10}Be data in the GISP2 ice core are reproduced in higher resolution in the data from the GRIP ice core with some rapid overprints, mainly in the ^{10}Be flux data. Although during rapid climate changes it is not clear which deposition is dominant[1], neither of both ^{10}Be concentration or ^{10}Be flux shows a pronounced $\sim 200 - 250$ years long anomaly comparable with the new Δ^{14}C data making a ^{14}C production rate change a very unlikely explaination (see also[25] for a discussion of difficulties linked to wet and dry deposition of ^{10}Be). Furthermore, upcoming new ^{10}Be data from the WAIS Divide Ice Core, Antarctica, show no abrupt changes around 14.6 kyr BP, excluding changes in ^{14}C production rate as a plausible cause for the Tahiti Δ^{14}C anomaly[26,27].

Supplementary Note 2

Evaluation of the Carbon Cycle Model. For model evaluation BICYCLE is (a) compared in its oceanic carbon uptake dynamic resulting in a model-specific airborne fraction with other models, (b) used to simulate the Suess effect (years $1820 - 1950$ AD), c) the bomb ^{14}C peak (years $1950 - 2000$ AD), and (d) applied on CO_2 release experiments for pre-industrial background conditions. The model is compared with results from another carbon cycle box model[15] (Suess effect and for pre-industrial conditions) and with output from the GENIE model[20], an Earth system model of intermediate complexity (pre-industrial conditions).

(a) Airborne fraction

A recent model inter-comparison[28] with 14 models (three comprehensive Earth System Models, seven Earth System Models of Intermediate Complexity, and four box-type models) calculated the airborne fraction f of an instantaneous CO_2 emission of 100 PgC to a background atmospheric CO_2 of 390 ppmv. We here repeat this scenario[28] by adding 100 PgC in year 2000 of our anthropogenic emission scenario (BICYCLE, terrestrial biosphere passive) having then a CO_2 of 389 ppmv. After year 2000 no further anthropogenic emissions are considered. The airborne fraction f is then calculated from the differences in atmospheric CO_2 for a run without this 100 PgC release (Supplementary Fig. 6d). f declines towards 0.45 after 100 years and to 0.20 after 1000 years, thus slightly larger than the rough estimate of $f = 0.17$ after 1000 years given previously[6], in which the experiment and background conditions were different. These results agree well with the model-mean of the model inter-comparison[28], which obtained $f = 0.41 \pm 0.13$ (2σ) and $f = 0.25 \pm 0.09$ after 100 and 1000 years, respectively. A smaller airborne fraction (faster oceanic uptake

rate) would allow a larger amount of carbon released to the atmosphere to be confined with ice core data.

(b) Suess effect

Further evaluation of the ^{14}C dynamics in BICYCLE was obtained from simulating the Suess effect[13,29]: the impact of anthropogenic fossil fuel and land use change emissions[10,11] on atmospheric Δ^{14}C (Supplementary Fig. 6a-c). This evaluation was chosen, because the Suess effect contains a well recognised influence of carbon emissions on atmospheric Δ^{14}C, which are of similar magnitude and duration as the carbon release we proposed for the onset of the B/A. We here apply the anthropogenic emission rates and use the BICYCLE model setup as previously published[30,31].

The pre-bomb Δ^{14}C data reconstructed from well dated tree-rings including the Suess effect[13] cover the years 1820–1950 with atmospheric Δ^{14}C decreasing from $+3‰$ to $-25‰$ (Supplementary Fig. 6c). In the original study[13] the Δ^{14}C data continue until the year 1954, however the reconstruction of the ^{14}C production rate[12] used for forcing the model stops at 1950, we therefore restrict our analysis also to results up to the year 1950. The Δ^{14}C data show especially a decline of $-23‰$ between 1900 and 1950, furthermore some multi-decadal feature before 1900. These atmospheric Δ^{14}C data contain the combined influence of the anthropogenic emissions and variations in the ^{14}C production rate on atmospheric Δ^{14}C. The cumulative anthropogenic carbon emissions during 1820–1950 sum up to 145 Pg of C (Supplementary Fig. 6a). Their ^{14}C signature depends on the relative share of ^{14}C-free fossil fuel emissions and land use change. For the latter we assume a Δ^{14}C signature of $-40‰$, being a mean value of pre-industrial terrestrial carbon within BICYCLE. Anthropogenic emissions were dominated until the beginning of the 20th century by land use change[11] with annual output of fossil fuels being only of secondary importance[10,32]. The assumed mean Δ^{14}C of the total anthropogenic emissions before 1850 was therefore only -40 to $-100‰$, but decreased to $-600‰$ around 1950 and $-750‰$ around 2000 (Supplementary Fig. 6a). We use the recent calculation of ^{14}C production rates based on changes in the geomagnetic field strength and the solar activity[12]. These relative ^{14}C production rates changes (calculated with respect to the long-term Holocene mean) varies in the two century from 1750 to 1950 between 82% and 112% (Supplementary Fig. 6a).

Most important features of the observed changes in atmospheric CO_2 rise and Δ^{14}C decline are met by our simulations. We focus on simulated changes, not absolute values, therefore all model simulations shown in Supplementary Figs. 6b,c are shown as anomalies to year 1820 (right y-axes). Absolute values of simulations results differed from reconstructions by less than 15 ppmv (CO_2) and less than 5‰ (Δ^{14}C).

Atmospheric CO_2 (Supplementary Fig. 6b) measured in the Law Dome ice core rises by 25 ppmv between 1820 and 1950. Results with BICYCLE find a 22 ppmv rise in the model version with active terrestrial biosphere for the same time period, implying that photosynthesis on land is via the fertilisation effect a function of atmospheric CO_2. If terrestrial carbon content is kept constant (passive terrestrial biosphere) the simulated rise in atmospheric CO_2 between 1820 and 1950 is 35 ppmv, 10 ppmv higher than in the ice core data.

Changes in atmospheric Δ^{14}C (Supplementary Fig. 6c) include both the rather steep decline after the year 1900, but also important multi-decadal features of the Δ^{14}C data consisting of a local maximum in Δ^{14}C around 1900, a declining trend before 1840 and rather stable values in-between. Those features are caused by corresponding anomalies in the ^{14}C production rates (Supplementary Fig. 6a). In the BICYCLE

simulations the steep declines in the first two decades and after year 1900 are met well, in the intermediate period of rather stable $\Delta^{14}C$, the model produces an offset with respect to the data of $3 - 5‰$. The difference in the two model applications with either active or passive terrestrial carbon cycle have only minor influence of $\sim 2‰$ on the simulated changes in atmospheric $\Delta^{14}C$. The model version with active terrestrial biosphere, which also compares best with changes in atmospheric CO_2, produces a decrease in atmospheric $\Delta^{14}C$ of $-28‰$ between 1820 and 1950 for the Suess effect (including natural variations in the ^{14}C production rates) which is in very good agreement with the data.

The overall model-data misfit for the time window $1820 - 1950$ is estimated from linear regression analysis of simulated changes against observed changes (Supplementary Fig. 7a,b). Here, only simulation results are picked for the n years in which observational data are available. An optimal model would have in such a scatter plot all points on the diagonal with slope $m = 1.0$. We here find for the simulated atmospheric CO_2 compared to the $n = 33$ data points of Law Dome regression coefficients m of the slopes of 1.07 and 0.70 BICYCLE with passive and active terrestrial biosphere, respectively. For changes in atmospheric $\Delta^{14}C$ ($n = 115$) the regression coefficients m of the slope are 1.10 and 1.00, listed again for the same simulation scenarios. These linear regression analyses led furthermore to $r^2 \geq 0.94$ for all model-data comparsions.

(c) Bomb ^{14}C peak

After the year 1950 the natural ^{14}C signals is overprinted by anthropogenic ^{14}C production during nuclear bomb testing. The so-called bomb ^{14}C peak will be used as an additional model evalution. The magnitude of the $\Delta^{14}C$ anomaly was by about a factor of 20 larger and faster than our carbon cycle anomaly during the onset of the B/A, but the data are still of use for analysing model dynamics.

Anthropogenic carbon emission in the setup for the Suess effect were already extended until year 2000 (Supplementary Fig. 6a). To investigate the bomb ^{14}C peak we need as additional forcing the bomb-induced artificial ^{14}C production. The background ^{14}C production rate varied before 1950 by 20% around the mean Holocene values (of here 440 mol yr^{-1}). From results of a ^{14}C budget closure[17] we calculate that the relative ^{14}C production rate increased in selected years (cyan points in Supplementary Fig. 6f). In the peak years $1960 - 1963$ this increase was by a factor of $30 - 84$. The cumulative additional ^{14}C production leads to the injection of $1.2 \cdot 10^6$g ^{14}C into the atmosphere after 1950. This is 15% smaller than intially[17] suggested, because our natural background ^{14}C production rate is only 85% of that chosen by Naegler[17].

The anthropogenic carbon emissions lead in the Law Dome[14] and Mauno Loa[16] data to a rise in CO_2 of 60 ppmv, from $\sim$310 ppmv in year 1950 to nearly 370 ppmv fifty years later (Supplementary Fig. 6e). The simulated CO_2 rise in BICYCLE (terrestrial biosphere active) is identical (slope $m = 1.0$ in data-model scatter plot (Supplementary Fig. 7c)), but offset by -15 ppmv. With passive terrestrial biosphere atmospheric CO_2 in BICYCLE rises faster leading to an amplitude of 85 ppmv, or a slope $m = 1.42$ in the data-model scatter plot.

The bomb ^{14}C peak was observed in the atmosphere at various station around the globe, and shows a distinct north-south gradient before the year 1970. The calculation of a global mean ^{14}C peak is therefore not straightforward. We here show a previously[18] calculated mean, but also the range of the data between high northern latitude and southern hemisphere (Supplementary Fig. 6f). The global mean in atmospheric $\Delta^{14}C$ peaks in the data in the mid 1960s at $700 \pm 200‰$, and declines towards $+100‰$ in year 2000

13

thereafter. Additional information can be gained from the rise in Δ^{14}C in corals, recording surface ocean signals. From a coral-data compilation[19] we show (Supplementary Fig. 6f) the range of results obtained in central equatorial Pacific surface waters, because these waters are less perturbed by upwelling or ocean gyres, and can be used for comparison with our simple carbon cycle box model. These coral data record the bomb ^{14}C peak by a rise from $-50‰$ in year 1950 towards $+100‰$ from year 1970 onwards.

BICYCLE simulates the bomb ^{14}C peak by an atmospheric Δ^{14}C of $+1000‰$ in year 1963, and a decay towards $0‰$ in year 2000. Results differ only slightly for terrestrial biosphere either active or passive. The model-data scatter plot (Supplementary Fig. 7d) shows a slope m of 1.09 and 1.14, and $r^2 = 0.79$ for both BICYCLE realisations. Simulated surface equatorial Pacific Δ^{14}C nicely shows the rise from 1950 to 1970 by $+150‰$ similar to the coral data, but simulations decline thereafter faster than in the data. The decay of the Δ^{14}C peak in atmosphere and surface ocean that is faster in the model than in the data indicates that the vertical mixing between surface and deep ocean in the model operates faster than in nature. This is a phenomenom well known for box models (in detail, the mixing in the high latitude is faster in box models than for GCMs, see the calculation of the Harvarton-Bear index[33,34], from which we quantified that this effect is less pronounced in BICYCLE than in other box models[34]). The effect is the more pronounced the larger the gradient in the tracers between surface and deep ocean is. The bomb ^{14}C peak is therefore only of limited usage for the evalution of the model dynamics of BICYCLE, when we want to apply the model to the B/A event, a problem with more than an order of magnitude smaller changes in the ^{14}C cycle.

(d) Carbon cycle model comparison

To obtain further knowledge on how the carbon cycle model performs and on how simulations depend on the specific chosen model setup and parametrization we repeat the Suess effect experiments with another carbon cycle box model[15] (Supplementary Fig. 6). Furthermore, CO_2 release experiments, similar to the release proposed by permafrost thawing around 14.6 kyr BP, but with pre-industrial background conditions are compared for both carbon cycle models, but also with output from the more complex GENIE model (Supplementary Fig. 8). This simplified setup is used as a sensitivity test under generic and comparable conditions.

The other box models have been used previously to study the influence of ^{14}C production changes[15] and thermohaline circulation changes[35]. Two geometries have been used with a 12 box model and a simpler 3 box model (V12b & V3b), which have been evaluated by calculating harmonic responses, in amplitude and phase, to sinusoidal changes of the ^{14}C production (previous studies[15,25] show a comparison with other models including the Bern2D model). V12b is a hybrid of PANDORA for the ocean[36] and the terrestrial part of the carbon cycle model of Siegenthaler[37]. V12b and V3b were updated to accommodate transient changes in the amount of ^{12}C in all reservoirs (assuming a constant Revelle buffer factor for ocean-atmosphere CO_2 exchanges). The airborne fraction after a thousand years for the 125 PgC release experiments is 0.18 and 0.11 for V3b and V12b, respectively. V3b is thus similar to the BICYCLE model, while version V12b has a carbon uptake faster than BICYCLE or most other models[28]. Sensitivity tests indicate that this problem is partly linked to the short residence time of carbon in the terrestrial biosphere (see below).

For the Suess effect, the time series forcing V12b and V3b (anthropogenic emissions, ^{14}C signature of emissions, natural changes in ^{14}C production) were identical to those forcing BICYCLE (Supplementary Fig. 6a). For the time interval 1820 to 1950 AD, the simulated atmospheric CO_2 rise is 17 and 30 ppmv for

V12b and V3b, respectively (Supplementary Fig. 6b). For the same 1820-1950 period, the atmospheric ^{14}C changes are -21 to $-24‰$ for V12b and V3b, respectively (Supplementary Fig. 6c). The carbon loss from the atmosphere being larger in V12b than in V3b, it is logical to observe that the CO_2 rise and atmospheric ^{14}C depletion are smaller in V12b than in V3b. Increasing the residence time of carbon in the terrestrial biosphere in V12b by a factor five (from 60 to 300 yr) leads to a total CO_2 increase by 24 ppmv and a ^{14}C depletion by $-23‰$ over the $1820 - 1950$ period.

Overall, Supplementary Figs. 6b and 6c show that for the Suess effect V12b and V3b compare well with BICYCLE results and with the CO_2 and Δ^{14}C observations. The slopes m in the model-data scatter plots (Supplementary Fig. 7a,b) are 0.93 (CO_2 V03b), 0.52 (CO_2 V12b), 0.85 (Δ^{14}C V03b) and 0.71 (Δ^{14}C V12b). In particular, V12b and V3b reproduce quite well the natural atmospheric Δ^{14}C variations before 1900 AD, mainly caused by geomagnetic field and solar activity. Some systematic differences are nonetheless observed: V12b underestimates by 10 ppmv the observed CO_2 rise and by $-5‰$ the ^{14}C depletion in 1950. Surprisingly, V3b matches quite well both observed datasets. As mentioned above, V12b performs better with a longer carbon residence time for its terrestrial biosphere. This effect is reminiscent to what is observed for BICYCLE: CO_2 observations are bracketed by simulations performed with a passive and active terrestrial biosphere, showing a difference of about 12 ppmv in 1950. BICYCLE slightly overestimate atmospheric Δ^{14}C changes linked to natural forcing.

The anthropogenic CO_2 release until year 2000 was also simulated with these box models, but not the bomb ^{14}C peak. First tests have shown that the post-bomb ^{14}C peak decay in atmospheric Δ^{14}C in those models is even faster than in BICYCLE, which again is very likely explained by vertical mixing parametrizations between surface and deep ocean. V03b and V12b increased their simulated atmospheric CO_2 between year 1950 and 2000 by about 70 and 40 ppmv, respectively (Supplementary Figs. 6e), leading to slopes m in scatter plot of 1.10 and 0.69 (Supplementary Fig. 7c).

We also performed a model comparison for a generic 125 PgC release over 50 or 200 years with pre-industrial background conditions. The ^{14}C signature of the released carbon was chosen to be $-1000‰$, i.e. ^{14}C-free carbon, equivalent to fossil fuel emissions. BICYCLE (with passive terrestrial biosphere) simulates CO_2 maxima of 37 and 25 ppmv, and Δ^{14}C minima of -55 and $-23‰$ for the 50 and 200 years release times, respectively (Supplementary Fig. 8). As expected from the Suess effect comparison, V3b produces CO_2 and Δ^{14}C changes almost as large as BICYCLE while V12b simulates anomalies that are a factor of two smaller. Again, using a longer biospheric residence time in V12b reduces partly the discrepancy (e.g. 23 ppmv and $-38‰$ instead of 18 ppmv and $-34‰$ for the 50 yr release).

For further evaluation these atmospheric carbon cycle perturbations under pre-industrial background conditions were also performed with GENIE, an Earth system model of intermediate complexity, in experiments without climate feedbacks to make them comparable to the box-models. The model configuration of GENIE for this experiment was as described earlier[20] with the addition of a ^{14}C source in the atmosphere that balances the steady-state ^{14}C decay in ocean and atmosphere. In the experiment with 50 years carbon release time the peak amplitudes of $\Delta(pCO_2)$ and $\Delta(\Delta^{14}$C) in GENIE are $+37$ ppmv and $-54‰$, respectively, so nearly identical to the results in BICYCLE (Supplementary Fig. 8a,c). For the experiment with 200 years release time the amplitudes in GENIE are with $+27$ ppmv ($\Delta(pCO_2)$) and $-26‰$ ($\Delta(\Delta^{14}$C)) slightly larger than in BICYCLE (Supplementary Fig. 8b,d). The decline of the atmospheric carbon anomalies in GENIE are more in agreement with the V03b box model, and slightly slower than in BICYCLE. This agrees with our findings that the airborne fraction f in BICYCLE is on a 100 years time scale comparable

with other models, but on a 1000 years time scale slightly smaller than the multi-model mean[28].

In summary, the comparison of the performances of BICYCLE, and the other models is a useful exercise of model evaluation, giving confidence in the BICYCLE simulations of older carbon cycle perturbations of similar amplitude and timing. We therefore conclude that our carbon cycle model is capable of simulating dynamics in the carbon and ^{14}C cycle of magnitude and duration of the Suess effect. For BICYCLE with passive terrestrial biosphere, the configuration used in the B/A experiments, the relative uncertainties in both CO_2 and Δ^{14}C are 7%, and 10%, respectively. The model thus seems to be a suitable tool for the investigation of the Δ^{14}C anomaly of similar characteristics around 14.6 kyr BP.

Supplementary Note 3

This Supplementary Note describes details of the climate simulations and analysis, which represents the basis for the discussion section that highlights the potential importance of abrupt GHG changes to offset the timing of the temperature maximum leading into the ACR, compared to the onset of the B/A.

(a) Data-based motivation

Ice core data and simulations show that the temperature signals connected with the bipolar seesaw are not uniform across Antarctica. Regional differences of millennial climate variability were found in Antarctic ice cores of different sectors during the last deglaciation[38,39] and MIS 3[40]. These earlier simulation results are not directly applicable for the climate transition around 14.6 kyr BP, because here we have to understand dynamics during an AMOC resumption.

The sequence of bipolar climate changes linking the onset of the B/A and the Antarctic Cold Reversal (ACR) is of particular interest for our study. However, rapid changes in CH_4 are used as age markers to synchronise ice cores from both hemispheres[41] leaving only the independently annual layer-counted chronologies of the WD ice core in the south and of NGRIP in the north for further investigations on the timing of the B/A and the ACR. Note, that temperature change[42] based on a stack from five East Antarctic ice cores (EDC, EPICA DML, Vostok, Dome Fuji, Talos Dome) shows the start of the ACR at approximately the same time as WD (Fig. 5, main text), although the underlying age model is not entirely independent from GICC05. If we analyse water isotopes from the two ice cores WD and NGRIP in detail they reveal a time delayed onset of $\sim$180 years in the ACR[38] relative to the beginning of the B/A[3,43], which is reduced to 145 years, once the Greenland temperature rise was aligned to 14.6 kyr BP. The given maximum counting uncertainties at the onset of the B/A are about 186 years for Greenland cores and 4% or 584 years for the ACR in WD. Note, that these uncertainty estimates already include and capture the suggestion that the GICC05 chronology might be at least 65 years too old around 12 kyr BP[44,45].

(b) Model setup

To test the importance of the abrupt carbon release and associated CO_2 changes for the temperature response in Antarctica we utilise the comprehensive Earth system model COSMOS in a coupled atmosphere-ocean configuration, consisting of ECHAM5[46] and MPI-OM[47] without any flux corrections[48]. The atmosphere

model ECHAM5 was used at T31 resolution ($\sim 3.75°$) with 19 vertical levels. The ocean model MPI-OM was run at an average resolution of $\sim 3°$ with 40 vertical layers. These model components have been applied for a wide range of glacial, interglacial and Neogene applications[8,49,50]. Furthermore, COSMOS has been evaluated with proxy data in an investigation of the LGM[9].

Based on the LGM ocean state and glacial boundary conditions we have performed two experiments in order to investigate the impact of abrupt CO_2 changes on the Antarctic temperature response. In experiment PRE_BA we have simulated 1200 model years to mimic a climate state that is characterised by GHG concentrations prior to the onset of the B/A. The respective concentrations are prescribed by constant values of CO_2 (228 ppmv), N_2O (233 ppbv) and CH_4 (498 ppbv) to represent conditions at $\sim$14.9 kyr BP (reference run). Additionally, we have used simulation PRE_BA as a basis to perform a transient simulation (CO2_ATM) with varying GHG concentrations after 600 years of model integration in PRE_BA.

In the transient experiment CO2_ATM we apply our suggested true atmospheric CO_2 spike of our best guess emission scenario (200 year long release of 0.625 Pg C yr^{-1} (in total 125 PgC) into the atmosphere resulting in a peak amplitude in atmospheric CO_2 change of 22 ppmv) together with measured N_2O [51] and Greenland CH_4 time series, the latter dated according to our understanding (Fig. 5 of main text). All GHG records as taken here are plotted in Supplementary Fig. 5. Using these GHG conditions, CO2_ATM has been run for 600 years. Hence, the two simulations can be used to deduce the impact of GHG changes at the inter-hemispheric temperature signature. Such a GHG forcing scenario seems to be reasonable as suggested by published (Fig. 3a of main text), CO_2 measurements, though absolute values in CO_2 might differ from the ones prescribed in our simulation CO2_ATM.

(c) Climate feedback interpretation

The application of the GHG forcing (Supplementary Fig. 5a) leads to a rise of the annual mean Antarctic surface temperature ΔT_{ANT} and the respective timing of the temperature evolution shows similarities with the temporal signature of the CO_2 forcing. The maximum warming of 0.6 K occurs about 250 years after the onset of the CO_2 rise (Supplementary Fig. 5a). The timing and estimated imprint of this temperature anomaly would generate about +0.5‰ changes in $\delta^{18}O$ if measured in Antarctic ice cores (assuming a slope in the water isotopic thermometer of 0.8‰ per K warming[52]). Based on the inter-hemispheric timing of the ACR in WD (but also in the ΔT_{ANT} stack from East Antarctic ice cores) we can derive that the apparent delay of the maximum isotopic value leading into the ACR with respect to the onset of the B/A in NGRIP can alternatively also be understood as a further increase of temperature and thus of $\delta^{18}O$ in WD (Fig. 5 of main text). The detected increase of $\sim$0.7‰ in WD suggests that the bulk of the observed signal might be explained by the simulated Antarctic temperature response to the abrupt increases in the GHG. The exact contribution will depend on the timing and the strength of the CO_2 pulse.

In this context the amplification of the AMOC at the end of Heinrich stadial 1 and associated temperature changes in Antarctica are of interest here. We thus compare our GHG forcing experiments with results on AMOC strengthening as obtained in previous model simulations using COSMOS[8,9] (Supplementary Fig. 5). Note, that most simulation studies focus on AMOC weakening[40,53]. Furthermore recently, it has been shown that the recovery and amplification of the AMOC in abrupt climate change simulations applying North Atlantic freshwater perturbations is strongly dependent on the climate background state[8]. Therefore, to evaluate the robustness of the Antarctic temperature response (ΔT_{ANT}) we analysed AMOC strenght-

ening for three different climate states that cover a wide spectrum of glacial-interglacial conditions (PI: pre-industrial; LGM: Last Glacial Maximum at 21 kyr BP; MIS3: 32 kyr BP). In these AMOC freshwater hosing experiments, explained in detail elsewhere[8,9], but briefly summarised in the caption to Supplementary Fig. 5, AMOC is weakened for about 150 years by the freshwater perturbation. Subsequently, the end of the freshwater input leads to AMOC resumption within 80–200 years. The magnitude and speed of the AMOC resumption depends on the climate background conditions (Supplementary Fig. 5b), as shown previously[8].

A comparison between the simulated influence of the GHG forcing and the freshwater hosing experiments highlights the relative importance of the GHG induced Antarctic temperature changes (lower panels in Supplementary Figs. 5a,b). As discussed above the GHG forcing might lead to a rise in ΔT_{ANT} of up to 0.6 K after 250 years, depending on the magnitude and timing of the CO_2 pulse. The freshwater hosing experiments are characterised by transient changes in ΔT_{ANT} of less than 0.3 K, starting from the time when freshwater input was shut off. In detail, ΔT_{ANT} depends on the background climate state. For example in the scenario with LGM background conditions ΔT_{ANT} was already rising prior to the freshwater shut-off due to transient changes. Furthermore, a comparison of the transient GHG scenario and the transient AMOC strengthening experiments shows that the ΔT_{ANT} response in the GHG simulation (Supplementary Fig. 5a) is stronger than the simulated impacts by AMOC changes (Supplementary Fig. 5b) already for GHG changes at the time when about half of the the full 22 ppmv increase in CO_2 is reached. Hence, also smaller GHG spikes bear the potential to have a substantial impact on the Antarctic temperature response when compared to effects caused by AMOC changes.

In summary, our model investigations suggest that the abrupt GHG changes are more important for the Antarctic temperature signature than changes associated with an abrupt AMOC strenghening. This highlights the potential of abrupt GHG changes to significantly modulate the Antarctic temperature signature during abrupt climate changes at the end of the last ice age.

Supplementary References

1. Finkel, R. C. & Nishiizumi, K. Beryllium 10 concentrations in the Greenland Ice Sheet Project 2 ice core from 3–40 ka. *Journal of Geophysical Research* **102**, 26699–26706 (1997).

2. Adolphi, F. *et al.* Persistent link between solar activity and Greenland climate during the Last Glacial Maximum. *Nature Geoscience* **7**, 662–666 (2014).

3. Rasmussen, S. O. *et al.* A new Greenland ice core chronology for the last glacial termination. *Journal of Geophysical Research* **111**, D06102 (2006).

4. Reimer, P. J. *et al.* IntCal13 and Marine13 Radiocarbon Age Calibration Curves 0–50,000 Years cal BP. *Radiocarbon* **55**, 1869–1887 (2013).

5. Durand, N. *et al.* Comparison of ^{14}C and U-Th ages in corals from IODP #310 cores offshore Tahiti. *Radiocarbon* **55**, 1947–1974 (2013).

6. Köhler, P., Knorr, G., Buiron, D., Lourantou, A. & Chappellaz, J. Abrupt rise in atmospheric CO_2 at the onset of the Bølling/Allerød: in-situ ice core data versus true atmospheric signals. *Climate of the Past* **7**, 473–486 (2011).

7. Köhler, P., Muscheler, R. & Fischer, H. A model-based interpretation of low frequency changes in the carbon cycle during the last 120 000 years and its implications for the reconstruction of atmospheric Δ^{14}C. *Geochemistry, Geophysics, Geosystems* **7**, Q11N06 (2006).

8. Gong, X., Knorr, G., Lohmann, G. & Zhang, X. Dependence of abrupt Atlantic meridional ocean circulation changes on climate background states. *Geophysical Research Letters* **40**, 3698–3704 (2013).

9. Zhang, X., Lohmann, G., Knorr, G. & Xu, X. Different ocean states and transient characteristic in Last Glacial Maximum simulations and implications for deglaciation. *Climate of the Past* **9**, 2319–2333 (2013).

10. Marland, G., Boden, T. & Andres, R. J. Global, Regional, and National CO_2 Emissions. In *Trends: A Compendium of Data on Global Change* (Carbon Dioxide Information Analysis Center, Oak Ridge National Laboratory, U.S. Department of Energy,, Oak Ridge, Tenn., USA, 2005).

11. Houghton, R. A. Revised estimates of the annual net flux of carbon to the atmosphere from changes in land use and land management 1850-2000. *Tellus* **55B**, 378–390 (2003).

12. Roth, R. & Joos, F. A reconstruction of radiocarbon production and total solar irradiance from the Holocene ^{14}C and CO_2 records: implications of data and model uncertainties. *Climate of the Past* **9**, 1879–1909 (2013).

13. Stuiver, M. & Quay, P. D. Atmospheric ^{14}C changes resulting from fossil fuel CO_2 release and cosmic ray flux variability. *Earth and Planetary Science Letters* **53**, 349–362 (1981).

14. Etheridge, D. M. *et al.* Natural and anthropogenic changes in atmospheric CO_2 over the last 1000 years from air in Antarctic ice and firn. *Journal of Geophysical Research* **D101**, 4115–4128 (1996).

15. Bard, E., Raisbeck, G. M., Yiou, F. & Jouzel, J. Solar modulation of cosmogenic nuclide production over the last millennium: comparison between ^{14}C and ^{10}Be records. *Earth and Planetary Science Letters* **150**, 453–462 (1997).

16. Keeling, R. F., Piper, S., Bollenbacher, A. & Walker, J. Atmospheric CO_2 records from sites in the SIO air sampling network. In *Trends: A Compendium of Data on Global Change.* (Carbon Dioxide Information Analysis Center, Oak Ridge National Laboratory, U.S. Department of Energy, Oak Ridge, Tenn., U.S.A., 2009). doi: `10.3334/CDIAC/atg.035`.

17. Naegler, T. & Levin, I. Closing the global radiocarbon budget 1945-2005. *Journal of Geophysical Research* **111**, D12311 (2006).

18. Hua, Q. & Barbetti, M. Review of tropospheric bomb C-14 data for carbon cycle modeling and age calibration purposes. *Radiocarbon* **46**, 1273–1298 (2004).

19. Grottoli, A. G. & Eakin, C. M. A review of modern coral $\delta^{18}O$ and $\Delta^{14}C$ proxy records. *Earth-Science Reviews* **81**, 67 – 91 (2007).

20. Cao, L. *et al.* The role of ocean transport in the uptake of anthropogenic CO_2. *Biogeosciences* **6**, 375–390 (2009).

21. Bard, E. Correction of accelerator mass spectrometry ^{14}C ages measured in planktonic foraminifera: Paleoceanographic implications. *Paleoceanography* **3**, 635–645 (1988).

22. Butzin, M., Prange, M. & Lohmann, G. Readjustment of glacial radiocarbon chronologies by self-consistent three-dimensional ocean circulation modeling. *Earth and Planetary Science Letters* **317 - 318**, 177 – 184 (2012).

23. Singarayer, J. S. *et al.* An oceanic origin for the increase of atmospheric radiocarbon during the Younger Dryas. *Geophysical Research Letters* **35**, L14707 (2008).

24. Kubota, K., Yokoyama, Y., Ishikawa, T., Obrochta, S. & Suzuki, A. Larger CO_2 source at the equatorial Pacific during the last deglaciation. *Scientific Reports* **4**, 5261 (2014).

25. Delaygue, G. & Bard, E. An Antarctic view of Beryllium-10 and solar activity for the past millennium. *Climate Dynamics* **36**, 2201–2218 (2011).

26. Woodruff, T., Welten, K., Caffee, M. & Nishiizumi, K. Cosmogenic ^{10}Be in WAIS Divide from 6–19 kyr BP. In *WAIS Divide Ice Core Science Meeting* (24–25 Sep 2013, La Jolla, CA, 2013).

27. Woodruff, T., Welten, K., Caffee, M. & Nishiizumi, K. Cosmogenic ^{36}Cl and ^{10}Be in the WAIS Divide ice core from 6–21 kyr BP. In *AGU Fall Meeting, Abstract C13A-0665* (9–13 Dec 2013, San Francisco, CA, 2013).

28. Joos, F. *et al.* Carbon dioxide and climate impulse response functions for the computation of greenhouse gas metrics: a multi-model analysis. *Atmospheric Chemistry and Physics* **13**, 2793–2825 (2013).

29. Suess, H. E. Radiocarbon Concentration in Modern Wood. *Science* **122**, 415–417 (1955).

30. Köhler, P., Fischer, H., Schmitt, J. & Munhoven, G. On the application and interpretation of Keeling plots in paleo climatic research — Deciphering $\delta^{13}C$ of atmospheric CO_2 measured in ice cores. *Biogeosciences* **3**, 539–556 (2006).

31. Köhler, P., Hartmann, J. & Wolf-Gladrow, D. A. Geoengineering potential of artificially enhanced silicate weathering of olivine. *Proceedings of the National Academy of Science* **107**, 20228–20233 (2010).

32. Andres, R. J. *et al.* A synthesis of carbon dioxide emissions from fossil-fuel combustion. *Biogeosciences* **9**, 1845–1871 (2012).

33. Broecker, W. *et al.* How strong is the Harvardton-Bear constraint? *Global Biogeochemical Cycles* **13**, 817–820 (1999).

34. Köhler, P., Fischer, H., Munhoven, G. & Zeebe, R. E. Quantitative interpretation of atmospheric carbon records over the last glacial termination. *Global Biogeochemical Cycles* **19**, GB4020 (2005).

35. Bard, E. *et al.* The North Atlantic atmosphere-sea surface ^{14}C gradient during the Younger Dryas climatic event. *Earth and Planetary Science Letters* **126**, 275 – 287 (1994).

36. Broecker, W. S. & Peng, T.-H. Carbon Cycle 1985: Glacial to interglacial changes in the operation of the global carbon cycle. *Radiocarbon* **28**, 309–327 (1986).

37. Siegenthaler, U., Heimann, M. & Oeschger, H. ^{14}C variations caused by changes in the global carbon cycle. *Radiocarbon* **22**, 177–191 (1980).

38. WAIS Divide Project Members. Onset of deglacial warming in West Antarctica driven by local orbital forcing. *Nature* **500**, 440–444 (2013).

39. Stenni, B. *et al.* Expression of the bipolar see-saw in Antarctic climate records during the last deglaciation. *Nature Geoscience* **4**, 46–49 (2011).

40. Buiron, D. *et al.* Regional imprints of millennial variability during the MIS 3 period around Antarctica. *Quaternary Science Reviews* **48**, 99 – 112 (2012).

41. Veres, D. *et al.* The Antarctic ice core chronology (AICC2012): an optimized multi-parameter and multi-site dating approach for the last 120 thousand years. *Climate of the Past* **9**, 1733–1748 (2013).

42. Parrenin, F. *et al.* Synchronous change in atmospheric CO_2 and Antarctic temperature during the last deglacial warming. *Science* **339**, 1060 – 1063 (2013).

43. Steffensen, J. P. *et al.* High-resolution Greenland ice core data show abrupt climate change happens in few years. *Science* **321**, 680–684 (2008).

44. Muscheler, R. *et al.* Tree rings and ice cores reveal ^{14}C calibration uncertainties during the Younger Dryas. *Nature Geoscience* **1**, 263 – 267 (2008).

45. Lohne, O. S., Mangerud, J. & Birks, H. H. Precise ^{14}C ages of the Vedde and Saksunarvatn ashes and the Younger Dryas boundaries from western Norway and their comparison with the Greenland Ice Core (GICC05) chronology. *Journal of Quaternary Science* **28**, 490–500 (2013).

46. Roeckner, E. *et al.* *The atmospheric general circulation model ECHAM5, part I: Model description*, vol. 349 of *Reports* (Max Planck Institute for Meteorology, Hamburg, Germany, 2003).

47. Marsland, S. J., Haak, H., Jungclaus, J. H., Latif, M. & Röske, F. The Max Planck Institute global ocean/sea ice model with orthogonal curvilinear coordinates. *Ocean Modelling* **5**, 91–127 (2003).

48. Jungclaus, J. *et al.* Ocean circulation and tropical variability in the coupled model ECHAM5/MPI-OM. *Journal of Climate* **19**, 3952–3972 (2006).

49. Knorr, G., Butzin, M., Micheels, A. & Lohmann, G. A warm Miocene climate at low atmospheric CO_2 levels. *Geophysical Research Letters* **38**, L20701 (2011).

50. Zhang, X., Lohmann, G., Knorr, G. & Purcell, C. Abrupt glacial climate shifts controlled by ice sheet changes. *Nature* **512**, 290–294 (2014).

51. Schilt, A. *et al.* Atmospheric nitrous oxide during the last 140,000 years. *Earth and Planetary Science Letters* **300**, 33 – 43 (2010).

52. Masson-Delmotte, V. *et al.* A Review of Antarctic Surface Snow Isotopic Composition: Observations, Atmospheric Circulation, and Isotopic Modeling;. *Journal of Climate* **21**, 3359–3387 (2008).

53. Kageyama, M. *et al.* Climatic impacts of fresh water hosing under Last Glacial Maximum conditions: a multi-model study. *Climate of the Past* **9**, 935–953 (2013).